New Advances in the Mathematical Modeling of the Continuous Bulk Process for the Production of High-Impact Polystyrene Using Multifunctional Initiators

María L. Laganá,[1] Emilio Berkenwald,[1] Pablo Acuña,[2] Javier Enríquez Medrano,[2] Graciela Morales,[2] Diana Estenoz[1,3]

[1]*Departamento de Ingeniería Química, Instituto Tecnológico de Buenos Aires (ITBA), Av. Madero 399, C.P., 1106, Buenos Aires, Argentina*

[2]*Centro de Investigación en Química Aplicada (CIQA), Bv. E. Reyna Hermosillo 140, C.P, 25294, Saltillo, Coahuila, Mexico*

[3]*Instituto de Desarrollo Tecnológico para la Industria Química, INTEC (Universidad Nacional del Litoral - CONICET), Güemes 3450, C.P., 3000, Santa Fe, Argentina*

New advances in the mathematical modeling of the bulk continuous high-impact polystyrene (HIPS) process are presented. The model consists of three modules that allow the simulation of: (1) a polymerization reactor train, (2) a devolatilization (DV) stage, and (3) structure–properties relationships. The model is based on a kinetic mechanism that includes thermal initiation, chemical initiation by sequential decomposition of a multifunctional initiator, propagation, transfer to monomer, transfer to rubber, termination by combination and re-initiation, as well as high temperature crosslinking and oligomer generation reactions. The present model is comprehensive from a kinetic perspective, since it can be used to simulate a HIPS process using initiators of any functionality and structure. The model is adjusted and validated using previously unpublished experimental data for bulk continuous HIPS polymerization in a pilot-scale plant. The experimental work includes a series of polymerizations using three different multifunctional initiators: (1) luperox-331 M80 (L331), (2) pinacolone diperoxide, and (3) diethyl ketone triperoxide. The pilot plant comprised the main stages of an industrial HIPS process: prepolymerization, finishing and DV. Theoretical results show a good agreement with the experimental measurements.

INTRODUCTION

High-impact polystyrene (HIPS) is a reinforced engineering thermoplastic with a rubbery disperse phase. In the industrial production process, styrene (St) is polymerized in bulk in the presence of about 6% in weight of dissolved polybutadiene (PB). This heterogeneous product consists of a polystyrene (PS) matrix containing dispersed rubber particles, which in turn contain PS occlusions typically exhibiting "salami" or "core-shell" morphologies. The graft copolymer (GC), generated during the process, is accumulated at the interface stabilizing the heterogeneous system and promoting development of the morphology [1,2]. The presence of an elastomer in the recipe confers the material an increased impact resistance (IR), without impairing the high tensile strength and ease of processing with respect to general purpose PS.

The industrial continuous bulk process for HIPS production comprises four main stages: dissolution, prepolymerization, finishing, and devolatilization (DV) [3]. In the first stage, the rubber is dissolved in the monomer at relatively low temperatures. During Prepolymerization, the morphology of the material is developed. This stage begins with the addition of a chemical initiator until 30–40% conversion. Termination is carried out at higher temperatures and with no agitation in order to preserve the morphology of the product. In the DV, the polymer is separated from the nonreacted monomer by applying vacuum and high temperature. This higher temperature at the end of the process promotes rubber crosslinking and oligomer formation. Although the basic process has been well studied, several aspects are still to be elucidated regarding the physicochemistry of the process, and the interrelationships between process variables, molecular and/or morphological characteristics, and final properties.

There is a growing technological interest in improving the quality of the material and enhancing the process efficiency through its design and optimization. In addition, the need to devolatilize on a cost-efficient basis together with the increasing number of restrictions on the acceptable volatile contents in polymers has led to increased attention towards understanding and optimizing this stage of the process [4].

As in various industrial free radical polymerization processes, the use of monofunctional initiators is limited due to the difficulty of achieving a good balance between process productivity and product properties [5]. Bifunctional initiators in HIPS production processes have been studied [6–8]. It was observed that said initiators allow both high productivity and high-molecular weights. Initiators with higher functionalities (tri- and tetra-functional) have been studied in the case of PS homopolymerization [9], as well as for HIPS production [10]. It was observed that the sequential decomposition of the initiators leads to significant increases in the rate of polymerization and high molecular weights. Depending on the initiator molecular structure, it may also introduce branching in the chains, leading to improvements in rheological and processing properties [11].

Most mathematical models for the bulk HIPS process assumed the reaction system to be homogeneous and allowed to simulate both batch [3,6,12–15] and continuous industrial processes [6,7,16,17]. Regarding the use of multifunctional initiators, very few mathematical models are reported in the literature and all of

Correspondence to: G. Morales; e-mail: graciela.morales@ciqa.edu.mx or D. Estenoz; e-mail: destenoz@santafe-conicet.gov.ar

DOI 10.1002/pen.25041

them consider batch reactors [8,15]. In Estenoz et al. [8] monofunctional, bifunctional and initiator mixtures were studied in a batch reactor. In our recent work [15], the performance of three multifunctional peroxide initiators in a bulk HIPS batch process was experimentally and theoretically investigated. A series of batch reactions was carried out using multifunctional initiators with varying functionality and structure. The theoretical work consisted of a mathematical model for bulk HIPS polymerization using multifunctional initiators that predicts the evolution of the main polymerization variables as well as the detailed molecular structure of the polymeric species and the melt flow index (MFI) of the obtained HIPS.

Despite the industrial relevance of the DV stage on the final product properties, it has not yet been included in mathematical models for the synthesis of HIPS. As regards DV models, transport phenomena mechanisms have been considered in several works, but no reactions kinetics have been included. Thermal degradation, oligomer formation and crosslinking mechanisms have not been considered [18–21]. These mechanisms occur at temperatures higher than 180°C and have been theoretically and experimentally studied for St polymerization [22–25]. From a technological standpoint, these high temperature reactions are of great importance during the DV stage. Although bibliographic material based on the study of DV in polymers is available, only a limited number of studies relate specifically to PS [18,19].

This work is the first attempt to develop a comprehensive mathematical model for the continuous process of HIPS production using multifunctional initiators. The model comprises integrated modules that simulate the polymerization train, DV stage and selected structure–properties relationships. The model allows the estimation of all global variables along the process as well as quality variables, such as swelling index (SI), MFI, oligomer content, and residual monomer of the final material. The model can be used to simulate the process with any mono- or multifunctional initiator, either lineal or cyclic, or mixtures thereof. New experimental data for continuous polymerization of St in the presence of PB using different peroxide initiators at a pilot plant scale was obtained to adjust and validate the model. The model is then used to theoretically study the use of multifunctional initiators and the effect of process conditions on the product final properties.

Simulation of systems involving multifunctional initiators involve multi-dimensional models, especially in cases where the full molecular structure is to be estimated. Chain length as well as functional group distributions are to be simulated for every reacting species, which may include radicals with several active sites in the same molecule (i.e. multiradicals).

Attempts at modeling complex reactions, such as scission or multiradical formation for other materials using either deterministic or stochastic models, such as Monte Carlo (MC) can be found in the literature [26,27]. The election depends basically of a personal choice. MC method is very useful in such cases, but can be more time consuming because they depend on the sample size and have the problem of fluctuations and noisiness due to stochastic variation [28]. Moreover, purely stochastic models can be challenging to incorporate into optimization routines, therefore limiting their simulation capabilities. In this work, a deterministic model was used to solve the mass balances for each species. For the re-initiation step, a probabilistic method based on random number generation was employed.

MATHEMATICAL MODELING

The mathematical model of the industrial HIPS production process consists of three sub-models: a polymerization model for the reactor train, a DV Model for the Devolatilizer and a Structure–Properties Model for the calculation of MFI and SI. Figure 1 shows a schematic representation of the inputs and outputs of the integrated sub-models.

Polymerization Model

For the modeling of the reactor train, a reactor model of a generic Continuous Stirred Tank Reactor (CSTR) was developed. It is based on the kinetic mechanism presented in Table 1, which includes initiation *via* a multifunctional initiator, thermal initiation, propagation, transfer to the monomer, transfer to the rubber, combination termination, and re-initiation. The model is an extension of our previous work for a batch reactor [15]. The following is considered: (1) at the temperatures employed, the initiators decompositions are due exclusively to sequential decomposition [5,9,29], (2) intra-molecular termination is negligible [8], (3) disproportion termination is negligible [30], (4) all peroxide groups in the initiator and the accumulated homo- and copolymers exhibit the same thermal stability [31], (5) because of the short lifetime of radicals, decomposition of undecomposed peroxide groups does not occur in radical molecules [8], (6) propagation and transfer reactions are unaffected by chain length or conversion [8], and (7) degradation reactions are negligible [32].

Assuming a pseudo-homogeneous bulk polymerization [8], the mathematical model of Appendix A was developed for a generic CSTR.

The proposed model does not include an energy balance. However, temperature variations can be simulated through the use of standard or modified Arrhenius expressions for the kinetic parameters [8,32]. The mathematical model consists of two modules:

1. The Basic module (Appendix A.1) allows the prediction of global chemical species (monomer, initiators, total radical species, unreacted butadiene units, and undecomposed peroxide groups). To this effect, the subset of *Eqs. A.1.1–11, A.1.21,* and *A.1.25–34* must be solved.
2. The Distributions module, which allows the estimation of all chemical species concentrations, characterized by their

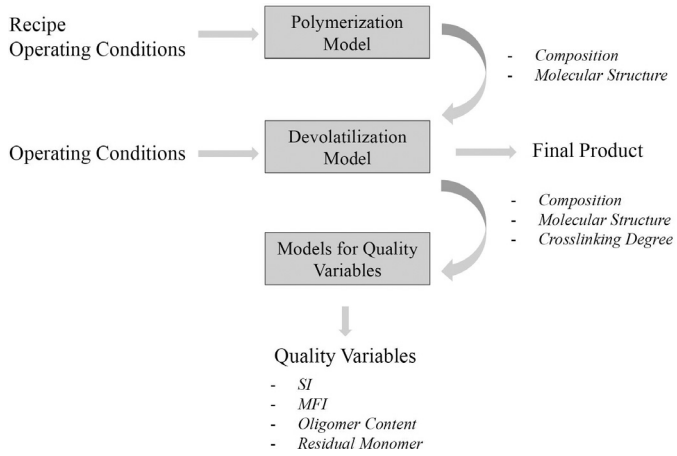

FIG. 1. Inputs and outputs diagram of the continuous HIPS production integrated sub-models. (1) Model for the polymerization reactor train, (2) model for the DV stage, and (3) models for final properties prediction.

TABLE 1. HIPS polymerization kinetic Mehanism.

Initiation (i = 0, 1, 2...)	
thermal initiation	$\cdot S_n \cdot^{(i)} + P^{(j)} 2k_{fG} S_n \cdot^{(i)} + P_0 \cdot^{(j)}$
$3St k_{i0} 2S_1 \cdot^{(0)}$	$P_0 \cdot^{(i)} + P^{(j)} k_{fG} P^{(i)} + P_0 \cdot^{(j)}$
Chemical initiation	$P_n \cdot^{(i)} + P^{(j)} k_{fG} P^{(i)} + P_0 \cdot^{(j)}$
$I^{(\varphi)} \varphi k_{d1} \cdot I \cdot^{(\varphi-1)}$	**Re-initiation**
	(n,l = 2, 3,...; m = 1, 2,..., n–1; i = l, 2,...; j = 0, l, 2... i–l)
$\bar{I}^{(\varphi)} \varphi k_{d1} I \cdot^{(\varphi-1)}$	$S_n^{(i)} i k_{d2} S_{n-m}^{(i-j)} \cdot + S_m^{(j)} \cdot$
$\cdot I \cdot^{(i)} + St 2k_{i1} \cdot S_1 \cdot^{(i)}$	$P^{(i)} i k_{d2} P_n^{(i-j)} \cdot + S_l^{(j)} \cdot$
$I \cdot^{(i)} + St k_{i1} S_1 \cdot^{(i)}$	**Combination termination**
$\cdot I \cdot^{(i)} + P^{(j)} 2k_{i2} P_0 \cdot^{(j)} + I \cdot^{(i)}$	(n, m = 1,2,3,$\cdots$; i, j = 0, 1, 2$\cdots$)
$I \cdot^{(i)} + P^{(j)} k_{i2} P_0 \cdot^{(j)} + \bar{I}^{(i)}$	
Propagation	
(n = 1,2,3,$\cdots$; i = 0, 1, 2$\cdots$)	$\cdot S_n \cdot^{(i)} + \cdot S_m \cdot^{(i)} 4k_{tc} \cdot S_{n+m}^{(i+j)} \cdot$
$S_n \cdot^{(i)} + St k_p S_{n+1} \cdot^{(i)}$	$\cdot S_n \cdot^{(i)} + S_m \cdot^{(j)} 2k_{tc} S_{n+m}^{(i+j)} \cdot$
$\cdot S_n \cdot^{(i)} + St 2k_p \cdot S_{n+1} \cdot^{(i)}$	$S_n \cdot^{(i)} + S_m \cdot^{(j)} k_{tc} S_{n+m}^{(i+j)}$
$P_0 \cdot^{(i)} + St k_{p0} P_1 \cdot^{(i)}$	$P_0 \cdot^{(i)} + P_0 \cdot^{(j)} k_{tc}^{'} P^{(i+j)}$
$P_n \cdot^{(i)} + St k_p P_{n+1} \cdot^{(i)}$	$P_0 \cdot^{(i)} + P_m \cdot^{(j)} k_{tc} P^{(i+j)}$
Transfer (n = 1, 2, 3, $\cdots$; i = 0, 1, 2$\cdots$)	$P_n \cdot^{(i)} + P_m \cdot^{(j)} k_{tc} P^{(i+j)}$
$S_n \cdot^{(i)} + St k_{fM} S_n^{(i)} + S_1 \cdot^{(0)}$	$P_0 \cdot^{(i)} + \cdot S_m \cdot^{(j)} + 2k_{tc}^{''} P_m^{(i+j)} \cdot$
$\cdot S_n \cdot^{(i)} + St 2k_{fM} S_n \cdot^{(i)} + S_1 \cdot^{(0)}$	$P_n \cdot^{(i)} + \cdot S_m \cdot^{(j)} + 2k_{tc}^{''} P_{n+m}^{(i+j)} \cdot$
$P_0 \cdot^{(i)} + St k_{fM}^{'} P^{(i)} + S_1 \cdot^{(0)}$	$P_0 \cdot^{(i)} + S_m \cdot^{(j)} + k_{tc}^{''} P^{(i+j)}$
$P_n \cdot^{(i)} + St + k_{fM} P^{(i)} + S_1 \cdot^{(0)}$	$P_n \cdot^{(i)} + S_m \cdot^{(j)} + k_{tc}^{''} P^{(i+j)}$
$S_n \cdot^{(i)} + P^{(j)} k_{fG} S_n^{(i)} + P_0 \cdot^{(j)}$	

chain length and number of undecomposed peroxide groups. The subset of *Eqs. A.2.1–9* and *A.2.12–14* estimate the complete MWD of each radical and polymer species, including free PS and residual PB. In order to consider the effect of re-initiation reactions in the MWDs, PS chains were assumed to have uniformly distributed peroxide groups. A random-chain scission is simulated with a uniformly distributed random variable. The uniform peroxide group distribution hypothesis is expected to be valid for cyclic initiators and for linear initiators with functionalities greater than two [33]. From the MWDs, the corresponding averages can be calculated using *Eqs. A.2.9–11*. A detailed description of the distributions module is presented in Appendix A.2.

The Basic module is solved using a Newton–Raphson method programmed in Matlab V. 8.3. The Distributions module is then solved using the results from the Basic module. In the Distributions module, a large number of equations (more than 500,000) must be simultaneously solved for the calculation of MWDs. Given the large number of species considered and the re-initiation reactions involved, these mass balances are solved using an iteration algorithm, also programmed in Matlab V. 8.3.

To account for the non-ideality of the reactors, each reactor is considered as a series of "n" CSTRs, where "n" is an adjustment parameter [3]. The simulation of the reactor train model involved the sequential resolution of each reactor in the train. Note that the Prepolymerization Reactor (R1), the Termination Reactor (R2), the Zapper Unit (ZU), and the last stage of the Devolatilizer are considered CSTR reactors. Predictions at the ZU outlet are used to feed the DV model.

DV Model

Polymer DV is a complex process that involves the transport of volatiles to a polymer-vapor interface, the evaporation of the volatiles at the interface and their subsequent removal by a vacuum system. DV progresses through a foaming mechanism: bubbles containing the volatiles to be removed are formed within the polymer melt. These bubbles may grow, coalesce and finally rupture at the polymer–vapor interface, releasing their volatile contents in the vapor phase. The crucial factors that determine the extent and rate of DV are the thermodynamics of the polymer–volatile system, the diffusion of the volatile through the polymer, and the nucleation and growth of vapor bubbles in the polymer melt [4,34].

With respect to DV equipment, the geometry of the Falling Strand Devolatilizer (FSD) employed in the pilot plant is shown in Fig. 2. The operation can be separated into two different stages. In the first stage, the polymer melt falls from a sprinkler forming strands that are in contact with the vapor phase. Bubbles nucleate, grow and break releasing the volatile components to the vapor phase, while chemical reactions take place in the melt. This "falling strand stage" in the FSD can be modeled as a plug flow reactor (PFR). The second stage, the "pool stage", involves the boiling polymer melt pool at the bottom of the FSD. As the boiling mechanism produces agitation, a CSTR model is adopted. At this stage, molecular diffusion is very shallow, as most bubbles are likely to be "buried" more rapidly by the falling melt than they can rise through the viscous melt pool. The bubbles therefore contract under the increasing melt head [4,35].

The following is assumed: (1) Vapor bubbles are in equilibrium with the melt at the interface [34–36], (2) Mass transfer mechanism: diffusion into bubbles with no interaction effects [35,37–40], (3) Bubbles expand against surface tension and viscous forces in a Newtonian fluid [40], (4) Vapor in bubble behaves as an ideal gas, (5) No resistance to mass transfer in the vapor phase, (6) The melt is considered a continuum, (7) DV takes place in the bubble growth regime [4,35], (8) No bubble coalescence, (9) Shallow diffusion in melt pool [4,35,39], and (10) Constant pressure and temperature operation: the evaporation of volatile components originates cooling that must be compensated by a heat source (e.g., the heat delivered by a heating fluid).

The model also considers chemical reactions in both stages of the FSD, such as monomer thermal initiation, propagation,

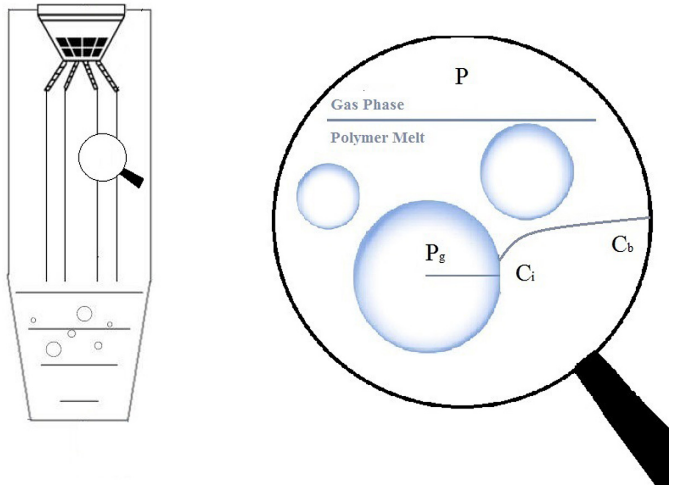

FIG. 2. Geometry of the FSD used in the pilot plant for all experiments (measures in cm) and mass transfer mechanism adopted for the mathematical model: Diffusion of volatiles into isolated bubbles in a continuous melt phase.

transfer to monomer, transfer to the rubber, termination, volatile species generation [36] (i.e., residual monomer, dimer, oligomer, etc.) and high-temperature crosslinking reactions [41].

In the PFR stage, the molar fluxes of the volatile species into the gas phase, considering equilibrium conditions, are calculated with *Eqs. B.1.1–4.* The Bubble growth mechanism for the flux calculation is based on the Rayleigh–Plesset Equation [40] for a bubble immersed in an infinite liquid and is presented in *Eq. B.1.19.* Then, the mass balances for the volatile and nonvolatile species in the melt phase can be used to calculate the corresponding concentrations using *Eq. B.1.5–13.* The total number of crosslinking points and the average molecular weight between crosslinks (M_C) are estimated using *Eqs. B.1.14–15.* For the Free PS MWD, *Eqs. B.1.16–18* are solved. Finally, mass balances for species in the gas phase are presented in *Eqs. B.1.21–25.*

In the pool stage, the mass balances in the polymer melt presented in *Eqs. B.1.16–18*, are solved considering only shallow diffusion [42,43]. The total number of crosslinking points and M_C are estimated using *Eqs. B.1.33–34.* For the MWDs, the same equations as in Appendix A.2 are used. The complete set of equations for this model is presented in Appendix B.

Structure–Properties Models

A mathematical model for prediction of the SI is presented [44]. The model considers: (1) Equivalent spherical gel, (2) Flory-Huggins theory for activity coefficients estimation, (3) No external osmotic pressure from diluted PS, (4) No contribution from interfacial tension, and (5) Simple strain energy function for a crosslinked network. The most relevant equations for this model are presented in Appendix C.

For the MFI estimation, the model reported in Luciani et al. [16] was employed. It is based on mass and momentum balances in a plastomer and assumes the following: (1) steady-state flow, (2) zero velocity at the capillary wall, and (3) the elongational viscosity can be estimated using Trouton's ratio. Although assumption (2) is valid for homogeneous systems [45], here it is extended to a heterogeneous one. In this model, the Weight Average Molecular Weight for free PS ($M_{w,PS}$) calculated in the Polymerization Module is used for the estimation of Polymer Melt and free PS viscosities.

EXPERIMENTAL

The experimental work consisted on a series of continuous bulk St polymerizations in the presence of dissolved PB, using the multifunctional initiators diethyl ketone triperoxide (DEKTP), pinacolone diperoxide (PDP), and L331 (Fig. 3) at 0.016% in weight. A 6% in weight of an alkyl lithium polymerized PB of medium cis –Diene 40 AC10- was dissolved into the monomer. The rubber was analyzed by size exclusion chromatography (SEC), and the average molecular weights resulted $\overline{M}_{n,PB} = 208,600$ g/mol and $\overline{M}_{w,PB} = 464,238$ g/mol. The polymerization recipe also included mineral oil to lower the viscosity of the solution and antirust to prevent rubber degradation. Some variations in the operating conditions were considered. In order to obtain different average molecular weights at the DV inlet, different temperatures in the Finishing Reactor were studied. In addition, in the FSD, both temperature and vacuum degree were varied. Conditions in the Prepolymerization Reactor were not altered and selected to achieve a proper steadying of the system and to ensure that phase inversion is achieved at this stage.

Reagents

The molecular structures of the initiators are shown in Fig. 3. L331 is a linear bifunctional initiator supplied by Sigma-Aldrich and was used as received. PDP and DEKTP, a cyclic bifunctional and a cyclic trifunctional initiator, respectively, were both synthesized in the laboratory as described in the following section.

The medium cis-PB was provided by Dynastol ElatomerosS.A de C.V., Mexico.

Monomer (St, 99.6%) was provided by Plastiformas (Monterrey, Mexico) with constant inhibitor level (10–28 ppm) verified by spectrophotometry according to ASTM D4590 and was used as received.

Toluene, Methanol (99.8%) and tetrahydrofuran (THF, ≥99%, HPLC grade) were supplied by Sigma-Aldrich and were used without further purification.

The mineral oil was supplied by Productos Químicos de Saltillo.

The untirust was Irganox 1,076 from BASF.

All Additives were used as received.

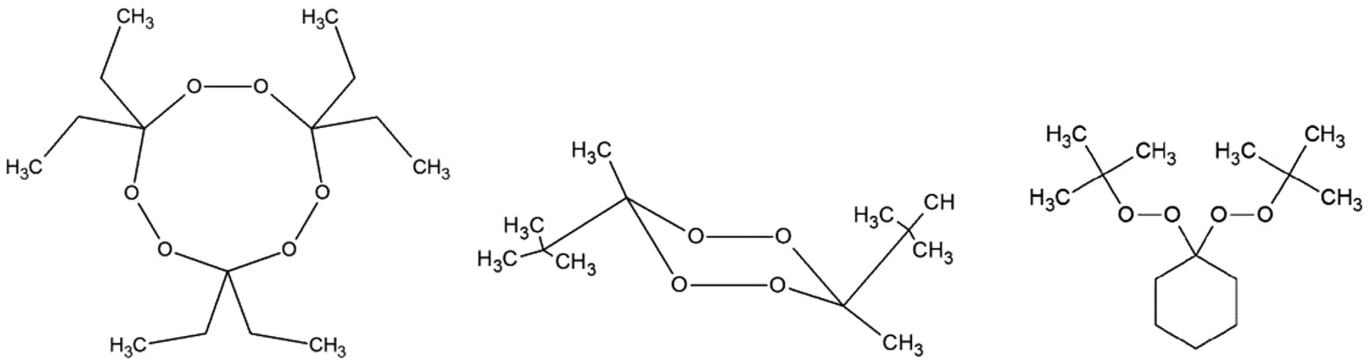

FIG. 3. Initiators molecular structures with their commercial and IUPAC names.

Initiators Synthesis

PDP was prepared according to methods previously described in the literature [1,26] The synthesis involves the reaction between 3,3-dimethyl-2-butanone and hydrogen peroxide (30% v/v) in sulfuric acid (70% v/v) at 15–20°C. DEKTP was also obtained according to methods reported in the literature [46]. Its synthesis involves the reaction between 3-pentanone and hydrogen peroxide (30% v/v) in sulfuric acid (70% v/v) at −15 to −20 °C. The purity of the peroxides was confirmed by nuclear magnetic resonance analysis.

Equipment and Operation

Figure 4 illustrates the pilot plant that was used for all experiments [47]. The prepolymerization stage is carried out in the first CSTR, reaching approximately 30% conversion. The operating temperature is typically not higher than 115°C. Termination takes place in a second CSTR, at higher temperatures. The selected polymerization temperatures are such that initiator decomposition is mostly sequential [48]. Finally, the DV stage takes place in a flash tank for the separation of low-molecular mass components under vacuum conditions and at elevated temperatures (i.e., 200–220°C). The plant also includes a ZU, the purpose of which is to lower the viscosity of the Devolatilizer inlet stream.

Upstream the train reactor, the rubber is dissolved at room temperature into the monomer in a semi-batch Dissolver Tank with the addition of a small amount of mineral oil. After 8 h of dissolution, its content is discharged into the Feed Tank and the chemical initiator and antirust are added. Table 2 summarizes the range of operating conditions for each stage.

Polymerization Process Conditions

The operating conditions selected for each experiment are presented in Table 3. Six experiments were carried out using L331 as initiator. In Experiments 1-a and 2-a, two different temperatures were considered for R2, to study the DV stage with two different average molecular weights inputs. In the FSD, both different temperatures and vacuum degrees were analyzed for reactions with L331. In this case, only results using L331 as initiator at 135°C in R2 are shown (i.e., Experiments 2-a/b/c/d). Additionally, a further experiment was carried out under the same reaction conditions as in Experiment 2-a, but varying the melt pool level in the Devolatilizer (i.e., Experiment 2-e). Finally, two further reactions were completed; one with PDP and another with DEKTP as initiators. Samples were taken at points S1–S4 as shown in Fig. 4.

TABLE 2. Equipment operating conditions and reaction volumes.

Equipment	Volume (L)	Operation T (°C)	Operation P (mmHg)
Disolver	24.1	21	760
Feed tank	2	21	760
R1	1.85	115	760
R2	1.1	125–135	760
Zapper	0.06	180–185	760
Devolatilizer	0.85–1.4	200–220	14–18

Characterization

Conversion (X), grafting efficiency (GE), and MWDs of free PS were measured for Samples S1–S4 in all experiments. For S3 and S4 samples, Monomer Content (%St) and Morphology were also determined. In addition, final product properties that is, MFI, SI, IR, and Elongation at Break (E) were determined in all the experiments.

X was determined by gravimetric analysis and the physical–chemical parameters (GE and SI) of different samples were measured directly from the pellets according to references 42,48.

Free PS MWD and the Free PS Average Molecular Weights ($M_{n,\ PS}$ and $M_{w,PS}$) were determined by SEC. A Hewlett-Packard instrument equipped with a series of three ultrastyrogel columns at porosities of 10^3, 10^4, and 10^5 Å was used. Calibration was carried out with PS standards (162–7,800,000 g/mol) and THF (HPLC grade) was used as eluent at a flow rate of 1 mL/min at 40°C.

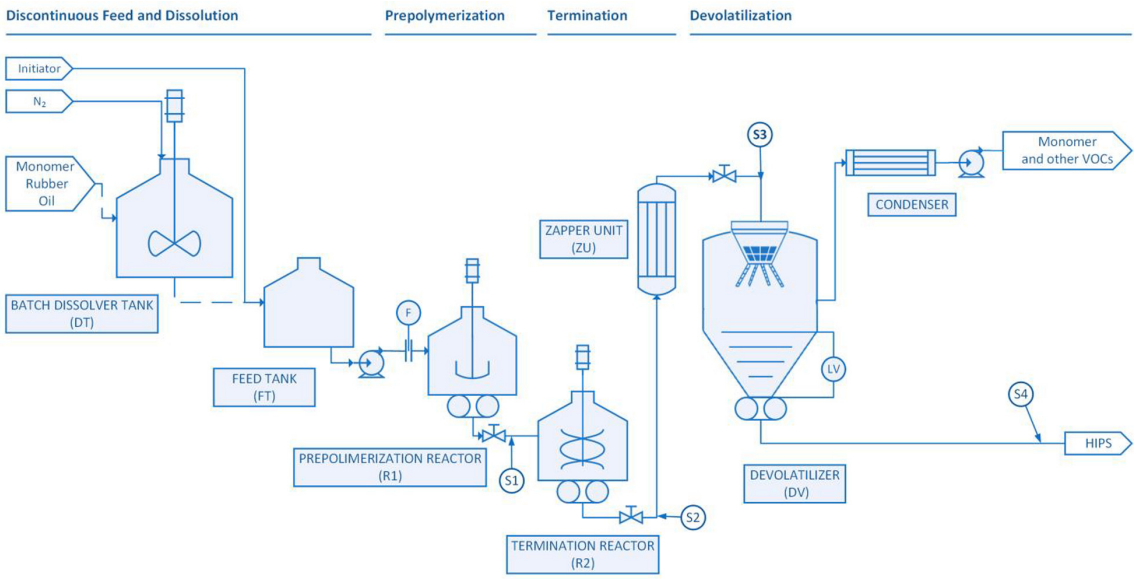

FIG. 4. Continuous bulk process for the production of HIPS. Pilot plant process flow diagram.

TABLE 3. Conditions adopted in the experiments for the study of HIPS production with three different multifunctional initiators.

Experiment	Initiator	TRl (°C)	TR2 (°C)	TDV (°C)	PDV[1] (mmHg)	Pool level DV (mm)
1-a	L-331	115	125	220	14–18	90
2-a	L-331	115	135	220	14–18	90
2-b	L-331	115	135	220	10–12	90
2-c	L-331	115	135	200	14–18	90
2-d	L-331	115	135	200	10–12	90
2-e	L-331	115	135	220	14–18	141
3	PDP	115	135	220	14–18	90
4	DEKTP	115	120/130[2]	220	14-18	90

[1] A pressure range is reported since vacuum in Devolatilizer resulted difficult to maintain stable.
[2] Two different temperatures are reported since the reaction was not stable during all the experiment duration.

The different morphological structures in the synthetized HIPS were observed by transmission electron microscopy (TEM). The samples were first cut to a thickness <100 nm with a diamond knife in a cryogenic ultra-microtome provided by Leica at a chamber temperature of −130°C, and −180°C. The obtained cuts were placed in a closed container and osmium tetroxide was added in order to stain and contrast the insoluble phase. Samples were left to stain for a period of 2 h. The Average Particle Diameters (Dp) were estimated from the micrographs using a public domain digital image processing program (ImageJ).

The MFI of the final product was determined following ASTM D-1238-13. An extrusion plastometer Dynisco Ph 800–332-224 was operated at 200 °C, and weighted with a 5 kg load.

The SI was determined by gravimetric analysis of 0.3 g of swelled sample. For the final product (material removed from the DV) the gel was solvated and swollen in toluene, and for the material obtained in R1, R2, and ZU, it was solvated and swollen in a solution of MEK/DMF (50/50).

IR was determined by Izod Impact Testing. First, the samples were processed to obtain test specimens by compression molding.

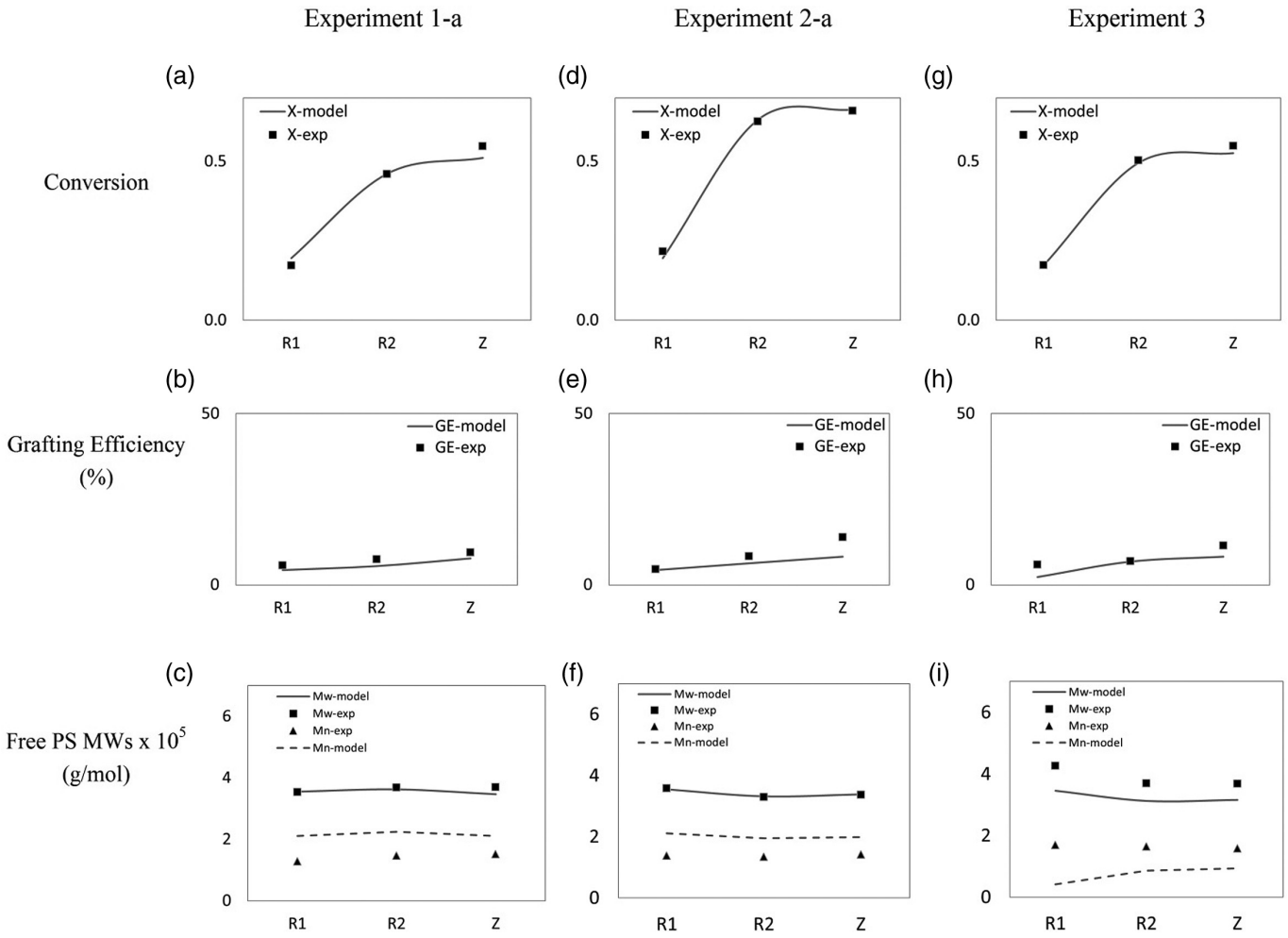

FIG. 5. Experimental results for polymerizations with L331 and PDP at different temperatures in R2.

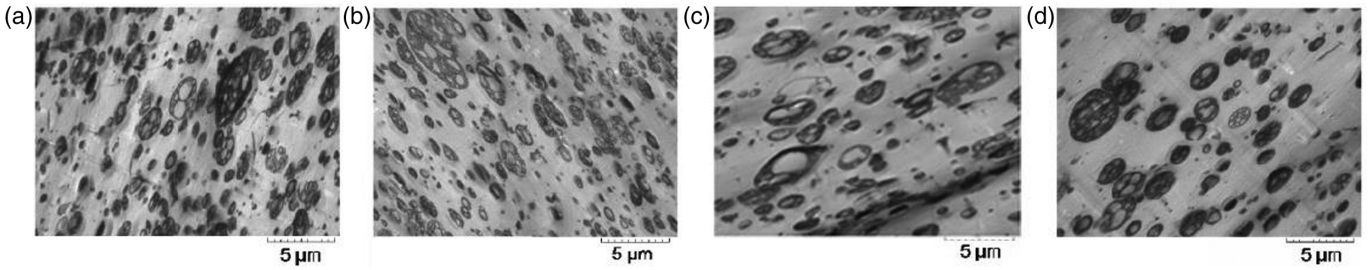

FIG. 6. Final product morphologies observed by TEM for polymerizations 1-a, 2-a, 3, and 4.

The test specimens were conditioned according to specifications required by standard ASTM D-256 (test specimens dimensions: 64 × 12.7 × 3.2 mm) and were subjected to an IZOD impact strength measurement. All measurements were made using a CSI equipment model 137 according to ASTM D-256 standard. Finally, E was determined according to ASTM-D 638–10. The test speed was 0.2 in/min and the separation between jaws was 4.5 in.

Experimental Results

Figure 5 shows the evolution of X, $M_{n,\ PS}$, $M_{w,PS}$ and GE along the reactor train for polymerizations using L331 as initiator at 125 and 135°C in R2 (Experiments 1-a and 2-a, respectively) and using PDP as initiator (Experiment 3). For DEKTP, only final properties were determined. In all cases, an increase of GE along the process is observed because of the temperature profile and addition of initiator. $M_{n,PS}$ and $M_{w,PS}$ are almost constant due to the opposite effects of the increase in temperature and the "gel effect". As expected, the increase in R2 temperature results in higher X, higher GE and lower $M_{n,PS}$ and $M_{w,PS}$ (Fig. 6a–f). When comparing the experimental results of L331 and PDP at the same conditions (Fig. 6d–i), the higher X for L331 can be attributed to a higher decomposition rate of the peroxide, as well as a higher initiator efficiency [43]. Further, the higher GE for L331 is associated to the higher rate of H-abstraction reactions by initiator radicals. As regards the molecular weights, it is observed that in the case of the cyclic initiator PDP, $M_{n,PS}$ and $M_{w,PS}$ are higher than in the case of the linear initiator L331, in accordance with a higher decomposition rate of the peroxide groups in L331 and the cyclic structure of the initiator, which generates di-radicals upon decomposition. These outcomes are consistent with what was found in our previous publications [15,33].

The main characteristics for experiments carried out at the same DV conditions are presented in Table 4 and Fig. 6. As expected, higher residual monomer content is found for reactions where lower conversions are obtained. In regards to oligomer generation reactions, they are affected both by monomer content and temperature. Thus, comparing reactions 1-a with 2-a, the lower oligomer content observed for the first is due to a lower oligomer generation rate, compensating the higher residual monomer content. In contrast, oligomer content for Experiment 2-a, carried out at the same temperature than Experiment 3, is lower due to the lower monomer concentration. MFI measurements corresponding to Experiments 1-a, 2-a, and 3 show higher values due to higher residual monomer content in spite of the slightly higher $M_{n,PS}$ and $M_{w,PS}$. Similarly, higher IR is obtained for experiments with higher monomer content, which acts as a plasticizer, enhancing mechanical properties [49]. Even though the same DV conditions were used, in experiments where monomer contents are higher at this stage, materials with higher SI are obtained. This is due to crosslinking reactions competing with propagation reactions, as it has been reported [41]. Finally, Fig. 6 shows the morphologies

TABLE 4. Final product quality variables for experiments with constant DV conditions (T = 220°C and P = 16 mmHg).

Exp	Mw (g/Mol)	GE (%)	Residual St (%)	Oligomer Cont.(%)	SI	MFI (g/10 min)	IR (J/m)	E(%)	Dp (nm)
1-a	288,358 (213060)	19.71 (14.74)	3.97(1.29)	1.38 (0.64)	15.85 (12.32)	6.5 (6.75)	264	13.7	1,056
2-a	268,338 (264420)	19.47 (13.00)	2.04(1.97)	1.43(1.02)	10.53 (12.36)	4.1 (4.32)	191	32.0	955
3	274,163 (269880)	17.15(8.25)	2.95 (2.97)	1.7 (2.71)	12.42 (12.36)	5.5 (4.16)	196	33.2	1,123
4	263,464 (240590)	16.35 (9.05)	1.10(3.42)	1.44 (3.47)	9.21 (12.31)	5.47 (5.22)	149	26.9	1,196

Simulation results are presented between parentheses.

TABLE 5. Final product properties at different DV conditions using L331 as initiator.

Exp.	$M_{n,PS}$ (g/Mol)	$M_{W,PS}$ (g/Mol)	GE (%)	SI	MFI (g/l0 min)	IR (J/m)	E (%)	Residual St (%)	Oligomer Content (%)
2-a	98,617 (103,640)	268,338 (264,420)	19.5 (13.00)	10.5 (12.36)	4.1 (4.32)	191 (202)	32.0 (44.2)	2.04 (1.97)	1.43 (1.02)
2-b	96,824 (104,620)	265,350 (264,380)	18.0(13.10)	9.3 (12.36)	5.6 (4.32)	156 (202)	27.1 (43.13)	2.11 (1.94)	1.65 (0.98)
2-c	107,493 (98,980)	265,825 (264,970)	18.8(9.30)	12.5 (12.36)	7.9 (4.31)	250 (203)	25.5 (49.7)	2.76 (3.47)	1.02 (1.13)
2-d	112,754 (100,190)	268,055 (264,930)	17.6 (9.41)	10.1 (12.36)	5.4 (4.31)	157 (203)	32.8 (48.3)	2.26 (3.40)	1.41 (1.08)
2-e	112,409 (103,650)	280,697 (265,950)	18.7 (11.86)	10.6 (12.31)	4.4 (4.27)	177 (202)	39.0 (44.8)	2.02(1.33)	1.67 (0.82)

Simulation results are presented between parentheses.

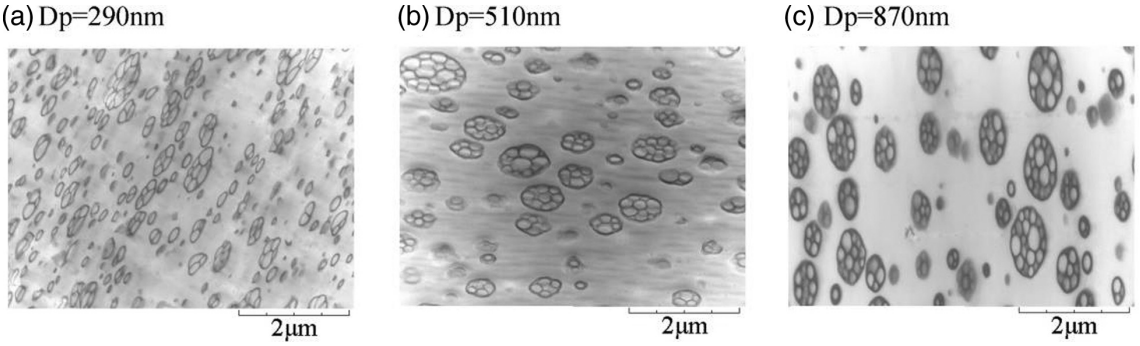

FIG. 7. Morphologies as observed by TEM for HIPS synthesized in a batch reactor with (a) L331, (b) PDP, and (c) DEKTP.

for the final materials. Larger number of particles with smaller Dp are observed for experiments with the linear initiator L331, in agreement with the higher measured GE. However, it should be noted that this variable is expected to have a large uncertainty due to the experimental technique [12]. Results for Experiment 4 are not discussed in this section since no intermediate data could be determined due to the difficult control of the reactor temperature. DEKTP final results are presented for their comparison to final results obtained using DEKTP in a batch reactor.

The characterizations of final products obtained using L331 as the initiator for the four different DV conditions studied are presented in Table 5. As expected, an increase in DV temperature reduces the residual monomer content of HIPS, which also results in a decreased IR, because of the monomer plasticizing function. As it can be observed in Experiments 2-c and 2-d, an increase in the vacuum degree enables reducing the residual monomer content, which also results in a decreased IR. The expected behavior with an increased vacuum degree was not obtained in Experiment 2-b, which suggests experimental errors associated to the poor stabilization of the applied vacuum, as was previously noted. Changes in DV temperature did not have a significant effect on the $M_{n,PS}$ and $M_{w,PS,}$ while the SI was lower at higher DV temperatures, indicating that crosslinking reactions are more important at this stage. Comparing Experiments 2-a and 2-e, the difference in the pool level does not result in significant changes in monomer content, indicating that all DV occurs in the very first portion of the "falling strand" stage, as it has been reported in several works [4,35,39]. All the important changes observed in the materials final properties for different conditions at the DV stage suggest that a strict control of this stage is essential to achieve the required product specifications.

Finally, Fig. 7 presents the morphologies of HIPS materials synthetized in a single batch reactor, using the initiators employed in the present work [15]. As the prepolimerization stage-where morphology is developed—has been held at similar conditions in both processes, it can be observed that products with smaller Dp are obtained with linear initiator L331 as compared with the cyclic initiators PDP and DEKTP for the batch reactor as well. Moreover, the morphology of materials obtained in a batch process present less dispersion, probably due to a better control of the morphology development.

TABLE 6. Polymerization and DV models parameters.

Parameter	Units	Expression or value	Reference
k_{d1},k_{dp} (L331)	s^{-1}	8.06 1011e–30,800.9/RT	Adjusted in this work
k_{d1}, k_{dp} (PDP)	s^{-1}	1.22 1010e–28,006.7/RT	Adjusted in this work
f_1, f_2 (L331)	—	1	Adjusted in this work
f_1, f_2 (PDP)	—	1	Adjusted in this work
k_{i0}	L^2/mol^2s	$1.1\ 10^5 e^{-13,810/T}$	[46]
k_{i1}, k_p	L/Mol s	$1.\ 051\ 10^7 e^{-7,067/RT}$	[50]
k_{i2} (L331)	L/Mol s	$2.13\ 10^3 e^{-5,867.6/RT}$	Adjusted in this work
k_{i2} (PDP)	L/Mol s	$3.05\ \mathbf{10^4 e^{-24,062.4/RT}}$	Adjusted in this work
k_{fM}	L/Mol s	7.28 104e–10,080.3/RT	Adjusted in this work
k_{fG}	L/Mol s	6.03 108e–17,311/RT	Adjusted in this work
k_{tc}	L/Mol s	$1.686109e^{-\left(\frac{844}{T}\right)-2\left(c_1\chi+c_2\chi^2+c_3\chi^3\right)}$ a	[46]
$D_{0,1}$	cm^2/s	5.0×10^{-3}	Adjusted in this work
$D_{0,2}$	cm^2/s	2.5×10^{-3}	Adjusted in this work
$D_{0,3}$	cm^2/s	1.7×10^{-3}	Adjusted in this work
N_r	l/cm^3	600	[49]
χ_{F-H}	—	0.28–0.33	[31,32]
k_D	L/Mol s	3.12 107e–25O971/RT	Adjusted in this work
k_T	L/Mol s	$1.35\ 10^6 e^{-21,907.6/RT}$	Adjusted in this work
A	—	1.8	[39]
B	—	1.35	[39]

[1] C_1 = 2.75–0.00505 T; C_2=-9.56–0.0176 T; C_3 = 3.03 + 0.00785 T. with χ monomer conversion.

SIMULATION RESULTS

The model was adjusted using the experimental data in Fig. 5. Model parameters are presented in Table 6. Parameter adjustment was sequential, using least-squares optimization algorithms. First, k_{d1} was adjusted with conversion data. It was assumed that $f_1 = f_2 = 1$. Subsequently, k_{i2}, k_{fM}, and k_{fG} were simultaneously adjusted with the average molecular weights and GE data. The values for initiator decomposition, transfer to monomer and transfer to rubber constants are within the range reported in the literature [8]. All other kinetic parameters were taken from the literature [32]. As regards the diffusion coefficients for volatile species, the obtained values after adjustment are in accordance with what has been reported [37,38]. All other parameters for the DV model were taken from the literature [34–36,39,40].

It was found in our previous publications [15,33] that f_1k_{d1} (L331) > f_1k_{d1} (DEKTP) and that k_{i2} (L331) > k_{i2} (DEKTP), by which the bifunctional linear initiator generates a higher number of grafting points at a given temperature. This result is in agreement with the lower grafting efficiencies observed for DEKTP compared with L331 and with the different morphologies observed in the final products.

Simulation results are compared with experimental results in Fig. 5, Tables 4 and 5 and a very good agreement between experimental and predicted values are observed.

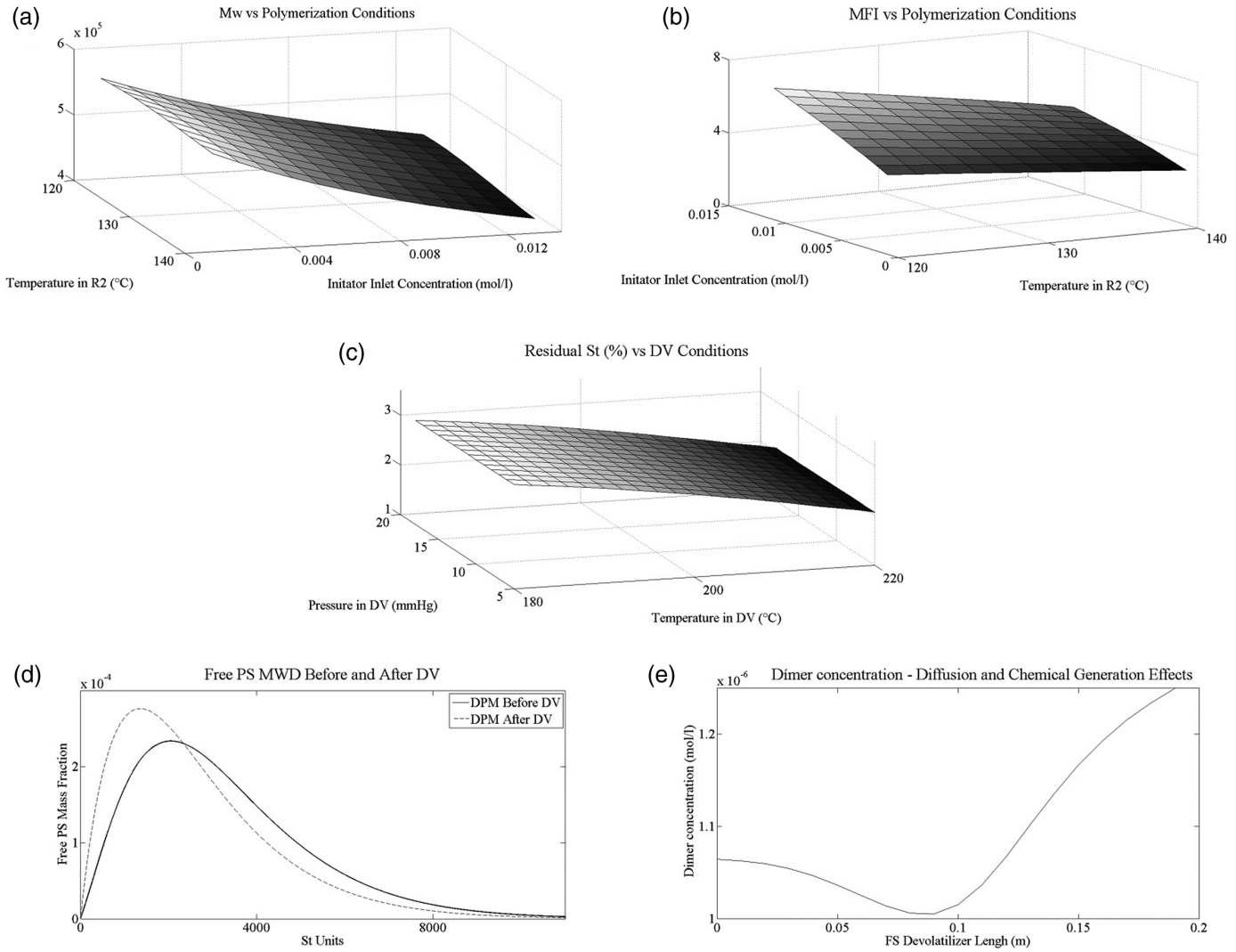

FIG. 8. Theoretical simulations for HIPS polymerization using multifunctional initiators in a continuous plant.

Other simulation results using the model are presented in Fig. 8. The model can be used to obtain smooth surfaces with predicted values of the final properties as function of any selected conditions at any stage of the process (Fig. 8a–c). In addition, variations in the molecular structure after the DV stage can be observed because of the generation of low molecular weight polymer, due to the high temperature, which promotes thermal initiation of the residual monomer (Fig. 8d). Moreover, Fig. 8e shows that, under the temperature and pressure conditions presented, when the length of the falling strand stage is increased by reducing the melt volume, there is evidence of opposite effects of mass transfer to the vapor phase and generation by chemical reaction related to the oligomer content in the final product.

CONCLUSIONS

An integrated mathematical model for the complete HIPS continuous polymerization process using multifunctional initiators was developed. An extensive experimental work was carried out in a continuous pilot plant to study the effects of operating conditions on final properties and structure–properties relationships. Each module of the model was adjusted and validated using these new experimental data. The integrated model can be used to simulate all stages of the continuous HIPS process including the DV stage. Furthermore, it is a comprehensive model, meaning it can be used with any mono- or multifunctional initiator, either linear or cyclic. The model provides a full insight into the molecular structure of the different polymer species (free PS, residual PB, and GC) and selected main quality variables, such as SI, MFI, oligomer content, and residual monomer.

The model was then used to theoretically study the effect of the recipe and operating conditions on the molecular structure and final properties of the obtained product.

The outcome of this work is a complete mathematical model structured by integrated modules that were developed from a deep understanding of the physical and chemical phenomena in each of the process stages. This model allows systematizing the interrelationships between operating conditions and final product quality for control and optimization of the overall production process.

The main long-term objective of this research line is to "invert" the model in order to find the optimum recipe and operating conditions to obtain tailor made products in an industrial continuous process.

The presented models could also be extended to other St polymers, such as SAN and ABS, or polymers from other monomers such as PMMA.

Nomenclature

- $S_1{\cdot}^{(i)}$ Monomer monoradical with *i* undecomposed peroxide groups
- $\cdot S_1{\cdot}^{(i)}$ Monomer diradical with *i* undecomposed peroxide groups
- $\bar{I}^{(\phi)}$ Linear multifunctional initiator with ϕ undecomposed peroxide groups
- $I^{(\phi)}$ Cyclic multifunctional initiator with ϕ undecomposed peroxide groups
- $I{\cdot}^{(i)}$ Initiator monoradical with *i* undecomposed peroxide groups
- $\cdot I{\cdot}^{(i)}$ Initiator diradical with *i* undecomposed peroxide groups
- $S_n^{(i)}$ Polymer with *n* repetitive units of St and *i* undecomposed peroxide groups
- $S_n{\cdot}^{(i)}$ PS monoradical of chain length *n* and *i* undecomposed peroxide groups
- $\cdot S_n{\cdot}^{(i)}$ PS diradical of chain length *n* and *i* undecomposed peroxide groups
- $P^{(i)}$ Copolymer with *i* undecomposed peroxide groups in the grafted chain
- $P_0{\cdot}^{(i)}$ Primary radical produced by attack to a butadiene repetitive unit (B) present in the residual PB or the $P^{(i)}$
- $P_n{\cdot}^{(i)}$ Copolymer radical with *i* undecomposed peroxide groups and n repetitive units of St in the active branch

APPENDIX A: POLYMERIZATION MODEL

BASIC MODULE

Balances for the Non-polymeric Reagents and Products

Multifunctional Initiators (ϕ = 1, 2, 3).

$$\frac{d}{dt}\left(\left[I^{(\phi)}\right]V\right) = -\phi k_{d1} f_1 \left[I^{(\phi)}\right]V + q_{in}\left[I^{(\phi)}\right]_{in} - q\left[I^{(\phi)}\right] \quad (A.1.1)$$

$$\frac{d}{dt}\left(\left[\bar{I}^{(\phi)}\right]V\right) = -\phi k_{d1} f_1 \left[\bar{I}^{(\phi)}\right]V + q_{in}\left[\bar{I}^{(\phi)}\right]_{in} - q\left[\bar{I}^{(\phi)}\right] \quad (A.1.2)$$

Secondary Initiator Species ($\phi > i$ = 1, 2).

$$\frac{d}{dt}\left(\left[\bar{I}^{(i)}\right]V\right) = -ik_{d1}\left[\bar{I}^{(i)}\right]V + (1-f_1)\sum_{j=i+1}^{\phi} jk_{d1}\left(\left[I^{(j)}\right] + \left[\bar{I}^{(j)}\right]\right)V + k_{i2}\left[\bar{I}{\cdot}^{(i)}\right]\left[B^*\right]V + q_{in}\left[\bar{I}^{(i)}\right]_{in} - q\left[\bar{I}^{(i)}\right] \quad (A.1.3)$$

Monomer

Assuming the "long chain approximation", by which propagation is the only monomer-consuming reaction:

$$\frac{d}{dt}([St]V) = -R_p V + q_{in}[St]_{in} - q[St] \quad (A.1.4)$$

where R_p is the global St polymerization rate,

$$R_p = k_p[St]([R\cdot] + 2[\cdot R\cdot]) \quad (A.1.5)$$

and

$$[R\cdot] = [S\cdot] + [P\cdot] = \sum_{i=0}^{\infty}\sum_{n=1}^{\infty}\left[S_n{\cdot}^{(i)}\right] + \sum_{i=0}^{\infty}\sum_{n=1}^{\infty}\left[P_n{\cdot}^{(i)}\right] \quad (A.1.6)$$

$$[\cdot R\cdot] = \sum_{i=0}^{\infty}\sum_{n=1}^{\infty}\left[\cdot S_n{\cdot}^{(i)}\right] \quad (A.1.7)$$

represent the total concentrations of mono- and diradicals respectively. In *Eq. A.1.6*, an S species is a PS homoradical, and a P species is a PB or copolymer radical.

Unreacted B units

Defining B* as an unreacted B unit in the copolymer or in the initial PB, its mass balance results:

$$\frac{d}{dt}\left(\left[B^*\right]V\right) = -\left\{k_{i2}\left[B^*\right]V + k_{fM}[St][P_0\cdot]V + q_{in}\left[B^*\right]_{in} - q\left[B^*\right]\right\} + k_{fG}([R\cdot] + 2[\cdot R\cdot])\left\{2\sum_{j=0}^{\phi-1}\left[\cdot I{\cdot}^{(j)}\right] + \sum_{j=0}^{\phi-1}\left(\left[I{\cdot}^{(j)}\right]\right)\right\} \quad (A.1.8)$$

with

$$[P_0\cdot] = \sum_{i=0}^{\infty}\left[P_0{\cdot}^{(i)}\right] \quad (A.1.9)$$

Radical Species (i = 0, 1, 2; n = 2, 3, …). Consider the mass balances of all free radical appearing in the global kinetics. Such balances provide:

$$\frac{d}{dt}\left(\left[\cdot I{\cdot}^{(i)}\right]V\right) = (i+1)f_1 k_{d1}\left[I^{(i+1)}\right]V - 2\left(k_{i1}[St] + k_{i2}\left[B^*\right]\right)\left[\cdot I{\cdot}^{(i)}\right]V + q_{in}\left[\cdot I{\cdot}^{(i)}\right]_{in} - q\left[\cdot I{\cdot}^{(i)}\right] \quad (A.1.10)$$

$$\frac{d}{dt}\left(\left[I{\cdot}^{(i)}\right]V\right) = p_j(i)f_2 k_{d2}\left[\bar{I}^{(j)}\right]V + 2k_{i2}\left[B^*\right]\left[\cdot I{\cdot}^{(i)}\right]V - \left(k_{i1}[St] + k_{i2}\left[B^*\right]\right)\left[I{\cdot}^{(i)}\right]V + q_{in}\left[I{\cdot}^{(i)}\right]_{in} - q\left[I{\cdot}^{(i)}\right] \quad (A.1.11)$$

$p_j(i)$ is the probability that the decompositions of the initiator of functionality *j* generates a monoradical with *i* undecomposed peroxide groups.

For PS homo radicals,

$$\frac{d}{dt}\left(\left[\cdot S_1{\cdot}^{(i)}\right]V\right) = 2k_{i1}\left[\cdot I{\cdot}^{(i)}\right][St]V - 2\left(k_p[St] + k_{fM}[St] + k_{fG}\left[B^*\right] + k_{tc}([R\cdot] + 2[\cdot R\cdot]) + k_{tc}^{''}[P_0\cdot]\right)\left[\cdot S_1{\cdot}^{(i)}\right]V + q_{in}\left[\cdot S_1{\cdot}^{(i)}\right]_{in} - q\left[\cdot S_1{\cdot}^{(i)}\right] \quad (A.1.12)$$

$$\frac{d}{dt}\left(\left[S_1{\cdot}^{(i)}\right]V\right) = k_{i1}\left[I{\cdot}^{(i)}\right][St]V - \left(k_p[St] + k_{fG}\left[B^*\right]\right) + k_{tc}([R\cdot] + 2[\cdot R\cdot]) + k_{tc}^{''}[P_0\cdot]\cdot\left[S_1{\cdot}^{(i)}\right]V + q_{in}\left[S_1{\cdot}^{(i)}\right]_{in} - q\left[S_1{\cdot}^{(i)}\right] + \delta_{i0}\left(2k_{i0}[St]^3 + k_{fM}([R\cdot] + 2[\cdot R\cdot] + k_{fM}[P_0\cdot])[St]\right) \quad (A.1.13)$$

(where δ_{i0} = 1 if i = 0 and δ_{i0} = 0 otherwise)

$$\frac{d}{dt}\left(\left[\cdot S_n \cdot^{(i)}\right]V\right) = 2k_p[St]\left(\left[\cdot S_{n-1} \cdot^{(i)}\right] - \left[\cdot S_n \cdot^{(i)}\right]\right)V$$
$$-2\left(k_{fM}[St] + k_{fG}\left[B^*\right] + k_{tc}([R\cdot] + 2[\cdot R]) + k_{tc}^{''}[P_0\cdot]\right)\left[\cdot S_n \cdot^{(i)}\right]V$$
$$+2k_{tc}\sum_{j=0}^{i}\sum_{m=1}^{n-1}\left[\cdot S_{n-m} \cdot^{(i-j)}\right]\left[\cdot S_m \cdot^{(j)}\right]V + q_{in}\left[\cdot S_n \cdot^{(i)}\right]_{in} - q\left[\cdot S_n \cdot^{(i)}\right] \tag{A.1.14}$$

$$\frac{d}{dt}\left(\left[S_n \cdot^{(i)}\right]V\right) = \left(k_p\left(\left[S_{n-1} \cdot^{(i)}\right] - \left[S_n \cdot^{(i)}\right]\right) + 2k_{fM}\left[\cdot S_n \cdot^{(i)}\right]\right)[St]V$$
$$+2k_{fG}\left[\cdot S_n \cdot^{(i)}\right]\left[B^*\right]V - \left(k_{fM}[St] + k_{fG}\left[B^*\right]\right.$$
$$\left.+k_{tc}([R\cdot] + 2[\cdot R]) + k_{tc}^{''}[P_0\cdot]\right)\left[S_n \cdot^{(i)}\right]V$$
$$+2k_{tc}\sum_{j=0}^{i}\sum_{m=1}^{n-1}\left[\cdot S_{n-m} \cdot^{(i-j)}\right]\left[S_m \cdot^{(j)}\right]V$$
$$+f_2k_{d2}\sum_{j=i+1}^{\infty}\sum_{m=n+1}^{\infty}\left(p_{mj}(n,i)j\left[S_m^{(j)}\right] + p_{mj}^{'}(n,i)j\left[P_m^{(j)}\right]\right)V$$
$$+q_{in}\left[S_n \cdot^{(i)}\right]_{in} - q\left[S_n \cdot^{(i)}\right] \tag{A.1.15}$$

In *Eq. A.1.15*, $p_{mj}(n, i)$ is the probability that a chain scission of dead polymer of length m and j peroxide groups yields a growing monoradical of chain length n with i peroxide groups, $p'_{mj}(n,i)$ is the probability that a chain scission of dead copolymer polymer of length m and i peroxide groups yields a growing monoradical of chain length n with i peroxide groups.

Adding this probability over all *i*s and *n*s, the following can be proved:

$$\sum_{i=1}^{\infty}\sum_{n=1}^{\infty}\sum_{j=i+1}^{\infty}\sum_{m=n+1}^{\infty}\left(p_{mj}(n,i)j\left[S_m^{(j)}\right] + p'_{mj}(n,i)j\left[P_m{}^{(j)}\right]\right)$$
$$=\sum_{i=1}^{\infty}\sum_{n=1}^{\infty}\left(2i\left[S_n^{(i)}\right] + i\left[P_n^{(i)}\right]\right) = 2[Pe_{PS}] + [Pe_C] \tag{A.1.16}$$

where $[Pe_{PS}]$ is the concentration of peroxide groups in the free PS chains and $[Pe_P]$is the concentration of peroxides groups in the copolymer. Note that the scission of any free PS chain with peroxide groups produces 2 PS monoradicals, whereas the scission of a chain within the copolymer generates only one PS monoradical and one copolymer monoradical.

For PB radicals and copolymer radicals, ($n \geq 2$).

$$\frac{d}{dt}\left(\left[P_0 \cdot^{(i)}\right]V\right) = k_{i2}\sum_{j=0}^{\phi-1}\left(2\left[\cdot I \cdot^{(j)}\right] + \left[I \cdot^{(j)}\right]\right) + k_{fG}([R\cdot] + 2[\cdot R])\Big)$$
$$\left[B^{*(i)}\right]V - \left(k_{p1}[St] + k'_{fM}[St] + k'_{tc}[P_0\cdot] + k_{tc}([R\cdot] + 2[\cdot R])\right)$$
$$\left[P_0 \cdot^{(i)}\right]V + q_{in}\left[P_0 \cdot^{(i)}\right]_{in} - q\left[P_0 \cdot^{(i)}\right] \tag{A.1.17}$$

$$\frac{d}{dt}\left(\left[P_1 \cdot^{(i)}\right]V\right) = k_{i1}[St]\left[P_0 \cdot^{(i)}\right]V + 2k_{tc}\sum_{j=0}^{i}\left[P_0 \cdot^{(i-j)}\right]\left[\cdot S_1{}^{(j)} \cdot\right]V$$
$$-\left(k_p[St] + k_{fM}[St] + k_{fG}\left[B^*\right] + k_{tc}^{''}[P_0\cdot] + k_{tc}([R\cdot] + 2[\cdot R])\right)\left[P_1 \cdot^{(i)}\right]V$$
$$+q_{in}\left[P_1 \cdot^{(i)}\right]_{in} - q\left[P_1 \cdot^{(i)}\right] \tag{A.1.18}$$

$$\frac{d}{dt}\left(\left[P_n \cdot^{(i)}\right]V\right) = k_p[St]\left[P_{n-1} \cdot^{(i)}\right]V + f_2k_{d2}\sum_{j=i+1}^{\infty}\sum_{m=n+1}^{\infty}p'_{mj}(n,i)j\left[P_m^{(j)}\right]V$$
$$+2k_{tc}\sum_{j=0}^{i}\sum_{m=1}^{n-1}\left[P_{n-m} \cdot^{(i-j)}\right]\left[\cdot S_m \cdot^{(j)}\right]V - \left(k_p[St] + k_{fM}[St] + k_{fG}\left[B^*\right] + k_{tc}^{''}[P_0\cdot]\right.$$
$$\left.+k_{tc}([R\cdot] + 2[\cdot R])\right)\left[P_n \cdot^{(i)}\right]V + q_{in}\left[P_n \cdot^{(i)}\right]_{in} - q\left[P_n \cdot^{(i)}\right] \tag{A.1.19}$$

where $[B^{*(i)}]$ is the molar concentration of total B units in PB or copolymer molecules with i = 0,1,2… undecomposed peroxide groups and.

A.1.20

$$\left[B^*\right] = \sum_{i=0}^{\infty}\left[B^{*(i)}\right] \tag{A.1.20}$$

Note that i = 0 for PB.

Summing *Eq. A.1.7* all over *i*s,

$$\frac{d}{dt}([P_0\cdot]V) = k_{i2}\sum_{j=0}^{\phi-1}\left(2\left[\cdot I \cdot^{(j)}\right] + \left[I \cdot^{(j)}\right]\right) + k_{fG}([R\cdot] + 2[\cdot R])\Big)\left[B^*\right]V$$
$$-\left(k_{i1}[St] + k'_{fM}[St] + k'_{tc}[P_0\cdot] + k_{tc}([R\cdot] + 2[\cdot R])\right)$$
$$[P_0\cdot]V + q_{in}[P_0\cdot]_{in} - q[P_0\cdot] \tag{A.1.21}$$

From *Eqs. A1.18, A1.19*, summing all over *n*s and *i*s, the total concentration of PB or copolymer homoradicals may be obtained:

$$\frac{d}{dt}([P\cdot]V) = k_{i1}[St][P_0\cdot]V + k_{d2}[Pe_C]V$$
$$-\left(k_{fM}[St] + k_{tc}^{''}[P_0\cdot] + k_{tc}([S\cdot] + [P\cdot])\right)[P\cdot]V + q_{in}[P\cdot]_{in} - q[P\cdot] \tag{A.1.22}$$

From *Eqs. A1.13, A1.15* and considering *Eq. A.1.6* the total concentration of PS monoradicals may be obtained:

$$\frac{d}{dt}([S\cdot]V) = k_{i1}\sum_{j=0}^{\phi-1}\left(\left[I \cdot^{(j)}\right]\right) + k_{fM}([P\cdot] + 4[\cdot R])\Big)[St]V + 2k_i[St]^3V$$
$$+2k_{fG}\left[B^*\right][\cdot R]V - \left(k_{tc}([S\cdot] + [P\cdot] + 2[\cdot R]) + k_{fG}\left[B^*\right] + k_{tc}^{''}[P_0\cdot]\right)$$
$$[S\cdot]V + f_2k_{d2}(2[Pe_{PS}] + [Pe_C])V + q_{in}[S\cdot]_{in} - q[S\cdot] \tag{A.1.23}$$

From *Eqs. A1.12, A1.14*, the total concentration of diradicals (which are only PS homoradicals) may be obtained:

$$\frac{d}{dt}([\cdot R\cdot]V) = k_{i2}\sum_{j=0}^{\phi-1}2\left[\cdot I \cdot^{(j)}\right][St]V + 2k_{tc}[\cdot R\cdot]^2V - 2\left(k_{fM}[St] + k_{fG}\left[B^*\right]\right.$$
$$\left.+k_{tc}([R\cdot] + 2[\cdot R]) + k_{tc}^{''}[P_0\cdot]\right)[\cdot R\cdot]V + q_{in}[\cdot R\cdot]_{in} - q[\cdot R\cdot] \tag{A.1.24}$$

The total radicals are calculated using *Eqs. A1.22, A1.23, A1.24*,

$$\frac{d}{dt}(([\mathrm{R}\cdot]+2[\cdot\mathrm{R}\cdot])V)=\left(k_{i1}\sum_{j=0}^{\phi-1}4\left[\cdot\mathrm{I}^{\cdot(j)}\right]+\left[\mathrm{I}^{\cdot(j)}\right]\right)[\mathrm{St}]V + 2k_i[\mathrm{St}]^3V+k_{i1}[\mathrm{St}][\mathrm{P}_0\cdot]V+2f_2k_{d2}([\mathrm{Pe_{PS}}] + [\mathrm{Pe_C}])V-k_{tc}([\mathrm{R}\cdot]+2[\cdot\mathrm{R}\cdot])^2V-k''_{tc}[\mathrm{P}_0\cdot]([\mathrm{R}\cdot]+2[\cdot\mathrm{R}\cdot]) + q_{in}\left([\mathrm{R}\cdot]_{in}+2[\cdot\mathrm{R}\cdot]_{in}\right)\text{-}q([\mathrm{R}\cdot]+2[\cdot\mathrm{R}\cdot]) \tag{A.1.25}$$

Peroxide Groups

Neglecting the concentration of peroxide groups in the radicals, the total concentration of peroxide groups is

$$[\mathrm{Pe}]=[\mathrm{Pe_I}]+[\mathrm{Pe_{PS}}]+[\mathrm{Pe_C}] \tag{A.1.26}$$

With

$$[\mathrm{Pe}_I]=\sum_{j=1}^{\phi}j\left(\left[\mathrm{I}^{(j)}\right]+\left[\bar{\mathrm{I}}^{(j)}\right]\right) \tag{A.1.27}$$

$$[\mathrm{Pe_{PS}}]=\sum_{i=0}^{\infty}\sum_{n=1}^{\infty}i\left[\mathrm{S}_n{}^{(i)}\right] \tag{A.1.28}$$

$$[\mathrm{Pe_C}]=\sum_{i=0}^{\infty}i\left[\mathrm{P}^{(i)}\right] \tag{A.1.29}$$

Where $[\mathrm{Pe_I}]$, $[\mathrm{Pe_{PS}}]$ and $[\mathrm{Pe_C}]$represent the molar concentration of peroxide groups accumulated in the initiator, the free PS and the copolymer, respectively.

Peroxide groups are consumes only by decomposition reactions. Therefore, it can be written

$$\frac{d}{dt}([\mathrm{Pe}]V)=-\sum_{j=1}^{\phi}jk_{d1}\left(\left[\mathrm{I}^{(j)}\right]+\left[\bar{\mathrm{I}}^{(j)}\right]\right)V-k_{d2}([\mathrm{Pe_{PS}}]+[\mathrm{Pe_C}])V + q_{in}[\mathrm{Pe}]_{in}\text{-}q[\mathrm{Pe}] \tag{A.1.30}$$

and,

$$\frac{d}{dt}([\mathrm{Pe}_I]V)=-\sum_{j=1}^{\phi}jk_{d1}\left(\left[\mathrm{I}^{(j)}\right]+\left[\bar{\mathrm{I}}^{(j)}\right]\right)V+q_{in}[\mathrm{Pe}_I]_{in}\text{-}q[\mathrm{Pe}_I] \tag{A.1.31}$$

Conversion and Volume

Monomer conversion can be calculated from

$$x=\frac{[\mathrm{St}]^0V^0-[\mathrm{St}]V}{[\mathrm{St}]^0V^0} \tag{A.1.32}$$

where the superscript "0" indicates initial conditions.

The evolution of the reaction volume V is obtained from

$$V=V_{\mathrm{St}}^0(1-\varepsilon x)+V_{\mathrm{PB}}^0 \tag{A.1.33}$$

with

$$\varepsilon=\frac{V_{\mathrm{St}}^0-V_{\mathrm{S}}^f}{V_{\mathrm{St}}^0} \tag{A.1.34}$$

where V_{St}^0 and V_{PB}^0 are the initial St and PB volumes respectively, $\varepsilon$is the St volume contraction factor and V_{S}^f is the final volume of free and grafted St at full conversion.

DISTRIBUTIONS MODULE

*PS Species (*i = *0, 1, …;* n = *2, 3, …)*

On the bases of the kinetic scheme presented in Table 1, the mass balance for each PS species can be derived.

$$\frac{d}{dt}\left(\left[\mathrm{S}_n{}^{(i)}\right]V\right)=k_{fM}[\mathrm{St}]\left[\mathrm{S}_n{}^{\cdot(i)}\right]V+k_{fG}\left[B^*\right]\left[\mathrm{S}_n{}^{\cdot(i)}\right] V+\frac{k_{tc}}{2}\sum_{j=0}^{i}\sum_{m=1}^{n-1}\left[\mathrm{S}_{n-m}{}^{\cdot(i-j)}\right]\left[\mathrm{S}_m{}^{\cdot(j)}\right]V-ik_{d2}\left[\mathrm{S}_n{}^{(i)}\right]V + (1-f_2)k_{d2}\sum_{j=i+1}^{\infty}\sum_{m=n+1}^{\infty}\left(p_{mj}(n,i)j\left[\mathrm{S}_m^{(j)}\right]+p'_{mj}(n,i)j\left[\mathrm{P}_m^{(j)}\right]\right)V + q_{in}\left[\mathrm{S}_n{}^{(i)}\right]_{in}\text{-}q\left[\mathrm{S}_n{}^{(i)}\right] \tag{A.2.1}$$

Let m be a uniformly distributed random variable whose value ranges from 1 to $n-1$. The polymer chain may form 2 monoradicals, one with length m, and the other one with length $n-m$. These chains will have $i-j$ and $j-1$ undecomposed peroxide groups, respectively. If the peroxide groups are assumed to be uniformly distributed within the polymer chains in the course of polymerization, the following relation must hold:

$$\frac{j-1}{n-m}=\frac{i-j}{m} \tag{A.2.2}$$

Therefore,

$$j=\left[\frac{i(n-m)+m}{n}\right] \tag{A.2.3}$$

where the brackets indicate the integer part of the expression.

The scission has then generated two monoradicals, one with length m and $i-j$ peroxide groups, the other one with length $n-m$ and $j-1$ peroxide groups.

Note that this chain scission algorithm can be modified for specific cases. For example, in the case of a linear bifunctional initiator, since all peroxide groups are located at a chain end, m = 1 for every scission.

The Number Chain Length Distribution (NCLD) for the free PS species is

$$N_{PS}^{(i)}(n)=q\left[\mathrm{S}_n{}^{(i)}\right] \tag{A.2.4}$$

found by integrating *Eq. A.2.1* with *Eqs. A1.14, A1.15* using also *Eqs. A1.12, A1.13* for species $[\cdot S_1{}^{\cdot(i)}]$ and $[S_1{}^{\cdot(i)}]$. The concentration for the total PS species characterized by the number of undecomposed peroxide groups can be calculated with

$$\left[P^{(i)}\right]=\sum_{n=1}^{\infty}\left[S_n{}^{(i)}\right] \tag{A.2.5}$$

The NCLD for the total polymer can be calculated using

$$P_n = \sum_{i=0}^{\infty} q\left[S_n{}^{(i)}\right] \tag{A.2.6}$$

The total moles of PS are

$$N_{PS} = \sum_{i=0}^{\infty}\sum_{n=1}^{\infty} N_{PS}^{(i)}(n) \tag{A.2.7}$$

To obtain the corresponding weight Chain Length Distribution (WCLD), multiply the NCLD by sM_{St} and replace n by s to obtain

$$G_{\mathrm{PS}}^{(i)}(s) = sM_{\mathrm{St}} q\left[\mathrm{S}_s{}^{(i)}\right] \tag{A.2.8}$$

The mass of Free PS can then be calculated as

$$G_{\mathrm{PS}} = \sum_{i=0}^{\infty}\sum_{s=1}^{\infty} G_{\mathrm{PS}}^{(i)}(s) \tag{A.2.9}$$

The average molecular weights can then be calculated from

$$\overline{M}_n = \frac{G_{\mathrm{PS}}}{N_{\mathrm{PS}}} = \frac{\sum_{i=0}^{\infty}\sum_{s=1}^{\infty} G_{\mathrm{PS}}^{(i)}(s)}{\sum_{i=0}^{\infty}\sum_{n=1}^{\infty} q\left[\mathrm{S}_n{}^{(i)}\right]} \tag{A.2.10}$$

$$\overline{M}_w = \frac{\sum_{i=0}^{\infty}\sum_{s=1}^{\infty} sG_{\mathrm{PS}}^{(i)}(s)}{G_{\mathrm{PS}}} = \frac{\sum_{i=0}^{\infty}\sum_{s=1}^{\infty} sG_{\mathrm{PS}}^{(i)}(s)}{\sum_{i=0}^{\infty}\sum_{s=1}^{\infty} G_{\mathrm{PS}}^{(i)}(s)} \tag{A.2.11}$$

Residual PB

$[n_{\mathrm{PB}}(b)]$denotes the molar concentration of unreacted PB with b units of B ($b \geq 1$). Assuming that the number of attacked B* is proportional to the B* contents of each chain length class, then the fraction of $P_0\cdot$ radicals that are primary PB radicals of chain length b is therefore$b[n_{\mathrm{PB}}(b)]/[\mathrm{B}^*]$. Then, from the kinetic mechanism the following balance is derived.

$$\frac{d}{dt}([n_{\mathrm{PB}}(b)]V) = -\left(k_{i2}\sum_{j=0}^{\phi-1}\left(2\left[\cdot I\cdot^{(j)}\right] + \left[\mathrm{I}^{(j)}\right]\right) + k_{fG}([\mathrm{R}\cdot] + 2[\cdot\mathrm{R}\cdot])\right) b[n_{\mathrm{PB}}(b)]V + k'_{fM}[\mathrm{St}][\mathrm{P}_0\cdot]\frac{b[n_{\mathrm{PB}}(b)]}{[\mathrm{B}^*]} + q_{in}[n_{\mathrm{PB}}(b)]_{in} - q[n_{\mathrm{PB}}(b)] \tag{A.2.12}$$

Where $[n_{\mathrm{PB}}(b)]_{in}$is known from experimental data.

The corresponding WCLD for the residual PB can be obtained from

$$G_{\mathrm{PB}}(b) = bM_{\mathrm{B}} q[n_{\mathrm{PB}}(b)] \tag{A.1.13}$$

The total moles and mass of the residual PB are therefore

$$N_{\mathrm{PB}} = \sum_{b=1}^{\infty} N_{\mathrm{PB}}(b) \tag{A.2.14}$$

$$G_{\mathrm{PB}} = \sum_{b=1}^{\infty} G_{\mathrm{PB}}(b) \tag{A.2.15}$$

GE and Grafting Density

The grafted St mass G_{GS}can be calculated from

$$G_{\mathrm{GS}} = M_{\mathrm{St}} q_{in}^0 [\mathrm{St}]_{in}^0 x - G_{\mathrm{PS}} \tag{A.2.16}$$

The St GE is calculated from

$$E_{\mathrm{GS}} = \frac{G_{\mathrm{GS}}}{G_{\mathrm{PS}} + G_{\mathrm{GS}}} \tag{A.2.17}$$

Phase volumes

The volumes of the individual phases, considered completely immiscible, is obtained from

$$V_I = \frac{G_{PB} + G_{GS}}{\rho_{PB}} \tag{A.2.18}$$

$$V_{II} = \frac{M_{St}[St]V_{II}\rho_{St} + G_{PS}}{\rho_{PS}} \tag{A.2.19}$$

APPENDIX B: DV MODEL

PFR STAGE

Mass balance in polymer melt

Diffusion Mechanism. The molar flux of a volatile species into the growing bubble $N_k$can be calculated on the base of classical penetration theory [48], corrected for convective effects due to bubble expansion [43]:

$$N_k = \sqrt{{}^{7}/_{3}}\left(\sqrt{{}^{D_k}/_{\pi\theta}} + {}^{D_k}/_{R}\right)(C_k - C_{in,k}) \tag{B.1}$$

where θ is the contact time of the fluid with the interphase, D_k is the solute mutual-diffusivity, which considers concentration gradients, R is the bubble radius, $C_{in,\ k}$is the solute concentration at the interphase, and $C_k$is the solute concentration in the bulk.

With k = St, Dm, Tm.

For the estimation of St diffusivity, the following expression based on the free volume theory is considered [29].

$$D_k = D_{0,k}\left(1 - \phi_k{}^2\right)(1 - 2\phi_k\chi) \tag{B.2}$$

Where $D_{0,\ k}$ is the solute self-diffusivity [44], $\phi_k$is the volume fraction of the solute in the melt, and $\chi$is the Flory-Huggins interaction parameter [31,32].

$\phi_k$is calculated as:

$$\phi_k = \frac{C_k MR_k}{\rho_k} \tag{B.3}$$

where $MR_k$is the molecular weight of the volatile species and $\rho_k$is the solute density.

Equilibrium condition. At equilibrium, the pressure of each volatile component in the vapor phase is equal to the vapor pressure of that species in the solution ($P_{g,\ k}$)and is calculated with the vapor pressure of the pure component $\left(P_k^0\right)$, considering a diluted solution in the DV [21,31]. Then, the following expression is derived.

$$w_{in,k} = \frac{y_k P_g \rho_k}{P_k^0 \rho_P e^{[1+\chi]}} \tag{B.4}$$

Where $w_{in,\ k}$is the weight fraction of the volatile species, $y_k$is the mole fraction of the volatile species in the vapor phase, $\rho_P$is the polymer density and $P_g$is the pressure inside the bubble, in equilibrium with the melt at the interphase.

A mass balance in a PFR for the volatile species in the melt phase gives,

$$\frac{dq}{dz} = -\sum_{k=1}^{3} N_k A_{in} \frac{N_r}{L} \frac{MR_k}{\rho_k} \tag{B.5}$$

$$q\frac{d[C_k]}{dz} + C_k \frac{dq}{dz} = -N_k A_{in} \frac{N_r}{L} + R_k A_T \tag{B.6}$$

$$R_M = -k_p[St][\mathrm{R}\cdot] - 2k_{i0}[St]^3 - 2k_D[St]^2 - 2k_T[St]^3 \tag{B.7}$$

$$R_{Dm} = 2k_{Dm}[St]^2 \tag{B.8}$$

$$R_{Tm} = 2k_{Tm}[St]^3 \tag{B.9}$$

Where A_{in} is the interfacial area of one bubble, $L$is the length of the equipment for this stage, N_r total number of bubbles in the melt.

For the nonvolatile species and crosslinking points,

$$\frac{d[\mathrm{R}\cdot]}{dz} = \frac{A_T}{q}\left(2k_{i0}[\mathrm{St}]^3 - k_{tc}[\mathrm{R}\cdot]^2 - k_{tc}{}''[\mathrm{R}\cdot][\mathrm{P}_0\cdot]\right) - [\mathrm{R}\cdot]\frac{1}{q}\frac{dq}{dz} \tag{B.10}$$

$$\frac{d[\mathrm{P}_0\cdot]}{dz} = \frac{A_T}{q}\left[k_{fG}[\mathrm{R}\cdot]\left[\mathrm{B}^*\right] - \left(k_{i1}[\mathrm{St}] + k'_{fM}[\mathrm{St}] + k'_{tc}[\mathrm{P}_0\cdot] + k_{tc}[\mathrm{R}\cdot]\right)[\mathrm{P}_0\cdot]\right] - [\mathrm{P}_0\cdot]\frac{1}{q}\frac{dq}{dz} \tag{B.11}$$

$$\frac{d\left[\mathrm{B}^*\right]}{dz} = \frac{A_T}{q}\left(k_{fM}[\mathrm{St}][\mathrm{P}_0\cdot] - k_{fG}[\mathrm{R}\cdot]\left[\mathrm{B}^*\right]\right) - \left[\mathrm{B}^*\right]\frac{1}{q}\frac{dq}{dz} \tag{B.12}$$

$$\frac{d[PeP]}{dz} = \frac{A_T}{q}\left(-f_{i2}k_{dp}[PeP]\right) - [PeP]\frac{1}{q}\frac{dq}{dz} \tag{B.13}$$

$$\frac{dN_X}{dz} = k_X[\mathrm{P}_0\cdot]^2 A_T \tag{B.14}$$

Where N_x is the number of crosslinks.

$$M_C = \frac{M_{n,PB}\cdot N_{PB,in}}{N_x} \tag{B.15}$$

Where M_c is the average molecular weight between crosslinks.

Free PS MWD.

$$\begin{aligned}\frac{d}{dt}\left(\left[\mathrm{S}_n\cdot^{(i)}\right]q\right) &= \left(k_p\left(\left[\mathrm{S}_{n-1}\cdot^{(i)}\right] - \left[\mathrm{S}_n\cdot^{(i)}\right]\right) + 2k_{fM}\left[\cdot\mathrm{S}_n\cdot^{(i)}\right]\right)[\mathrm{St}]A_T + 2k_{fG}\left[\cdot\mathrm{S}_n\cdot^{(i)}\right]\left[\mathrm{B}^*\right]A_T \\ &- \left(k_{fM}[\mathrm{St}] + k_{fG}\left[\mathrm{B}^*\right] + k_{tc}([\mathrm{R}\cdot] + 2[\cdot\mathrm{R}\cdot]) + k_{tc}^{''}[\mathrm{P}_0\cdot]\right)\left[\mathrm{S}_n\cdot^{(i)}\right]A_T \\ &+ 2k_{tc}\sum_{j=0}^{i}\sum_{m=1}^{n-1}\left[\cdot\mathrm{S}_{n-m}\cdot^{(i-j)}\right]\left[\mathrm{S}_m\cdot^{(j)}\right]V\end{aligned} \tag{B.16}$$

$$\begin{aligned}\frac{d}{dz}\left(\left[\cdot\mathrm{S}_n\cdot^{(i)}\right]q\right) &= 2k_p[\mathrm{St}]\left(\left[\cdot\mathrm{S}_{n-1}\cdot^{(i)}\right] - \left[\cdot\mathrm{S}_n\cdot^{(i)}\right]\right)A_T \\ &- 2\left(k_{fM}[\mathrm{St}] + k_{fG}\left[\mathrm{B}^*\right] + k_{tc}([\mathrm{R}\cdot] + 2[\cdot\mathrm{R}\cdot]) + k_{tc}^{''}[\mathrm{P}_0\cdot]\right)\left[\cdot\mathrm{S}_n\cdot^{(i)}\right]A_T \\ &+ 2k_{tc}\sum_{j=0}^{i}\sum_{m=1}^{n-1}\left[\cdot\mathrm{S}_{n-m}\cdot^{(i-j)}\right]\left[\cdot\mathrm{S}_m\cdot^{(j)}\right]A_T\end{aligned} \tag{B.17}$$

$$\begin{aligned}\frac{d}{dz}\left(\left[\mathrm{S}_n^{(i)}\right]q\right) &= k_{fM}[\mathrm{St}]\left[\mathrm{S}_n\cdot^{(i)}\right]A_T + k_{fG}\left[B^*\right]\left[\mathrm{S}_n\cdot^{(i)}\right]A_T \\ &+ \frac{k_{tc}}{2}\sum_{j=0}^{i}\sum_{m=1}^{n-1}\left[\mathrm{S}_{n-m}\cdot^{(i-j)}\right]\left[\mathrm{S}_m\cdot^{(j)}\right]A_T - ik_{d2}\left[\mathrm{S}_n^{(i)}\right]A_T\end{aligned} \tag{B.18}$$

The NCLD for the free PS species is obtained as it was described in Appendix A.2.

Bubble growth mechanism. By means of the Rayleigh–Plesset Equation for a bubble immersed in an infinite liquid and neglecting inertial and accelerations terms leads to [49]:

$$P_g - P = \frac{2\sigma}{R} + \frac{4\mu}{R}\frac{dR}{dt} \tag{B.19}$$

where, σ is the interfacial tension, μ is the viscosity, and P is the equipment operation pressure.

For this derivative to be positive, the following condition for bubble growth shall be considered:

$$P_g - P \geq \frac{2\sigma}{R} \tag{B.20}$$

Mass balance in the gas phase.

Assuming that a vapor in bubble behaves as an ideal gas and considering spherical bubbles,

$$P_g{}^4/_3\pi R^3 N_r = \dot{n}_g R_g T \tag{B.21}$$

where $\dot{n}_g$ is molar gas flow and $R_g$is the gas constant.

And a total mass balance in the gas phase assuming that no chemical reactions occurs gives,

$$d\frac{\dot{n}_g}{dz} = \sum_{k=1}^{3} N_k A_{in} \frac{N_r}{L} \tag{B.22}$$

Now, deriving *Eq. B.21* and combining with *Eq. B.22*,

$$\frac{dP_g}{dz} = \sum_{k=1}^{3} N_k 3\frac{R_g T}{RL} - \frac{3}{R}P_g\frac{dR}{dz} \tag{B.23}$$

For a volatile species k (k = *St, Dm, Tm*)

$$P_{g,k} = P_g \frac{\dot{n}_{g,k}}{\dot{n}_g} \tag{B.24}$$

$$d\frac{\dot{n}_{k,g}}{dz} = N_k A_{in} \frac{N_r}{L} \tag{B.25}$$

CSTR stage

Mass balance in polymer melt.

$$[St] = \frac{[St]_{in}{}^{*} q_{in} - N_{b1} A_{in} + V\left(-2k_p[\mathrm{St}][\mathrm{R}\cdot] - 2ki0[\mathrm{St}]^3 - 2k_D[\mathrm{St}]^2 - 3k_T[\mathrm{St}]^2\right)}{q} \tag{B.26}$$

$$[Dm] = \frac{[Dm]_{in}{}^{*} q_{in} - N_{b2} A_{in} + V k_D[\mathrm{St}]^2}{q} \tag{B.27}$$

$$[Tm] = \frac{[Tm]_{in}{}^{*} q_{in} - N_{b2} A_{in} + V k_T[\mathrm{St}]^3}{q} \tag{B.28}$$

$$[\mathrm{R}\cdot] = \frac{[\mathrm{R}\cdot]_{in}{}^{*} q_{in} + V\left(2k_{i0}[\mathrm{St}]^3 - k_{tc}[\mathrm{R}\cdot]^2 - k_{tc}{}''[\mathrm{R}\cdot][\mathrm{P}_0\cdot]\right)}{q} \tag{B.29}$$

$$[\mathrm{P}_0\cdot] = \frac{[\mathrm{P}_0\cdot]_{in}{}^{*} q_{in} + V\left[k_{fG}[\mathrm{R}\cdot]\left[\mathrm{B}^{*}\right] - \left(k_{i1}[\mathrm{St}] + k'_{fM}[\mathrm{St}] + k'_{tc}[\mathrm{P}_0\cdot] + k_{tc}[\mathrm{R}\cdot]\right)[\mathrm{P}_0\cdot]\right]}{q} \tag{B.30}$$

$$\left[\mathrm{B}^{*}\right] = \frac{\left[\mathrm{B}^{*}\right]_{in} q_{in} + V\left(k_{fM}[\mathrm{St}][\mathrm{P}_0\cdot] - k_{fG}[\mathrm{R}\cdot]\left[\mathrm{B}^{*}\right]\right)}{q} \tag{B.31}$$

$$[PeP] = \frac{[PeP]_{in} q_{in} + V\left(-f_{i2} k_{dp}[PeP]\right)}{q} \tag{B.32}$$

$$N_x = N_{x,in} + k_X[\mathrm{P}_0\cdot]^2 V \tag{B.33}$$

$$M_C = \frac{M_{n,PB} \cdot N_{PB,in}}{N_x} \tag{B.34}$$

APPENDIX C: SI MODEL

A spherical equivalent gel is proposed. Phase equilibrium conditions are written as radial and circumferential tensions balances [34].

The activity coefficients are estimated by the Flory-Huggins theory and molecular weight between crosslinks is previously calculated from the DV Model.

$$\ln(1-\phi_R) + \phi_R + \chi_R \phi_R{}^2 + \frac{\rho_R V_1 \phi_R{}^{1/3}}{M_C K^{4/3}} = 0 \tag{C.1}$$

$$\ln(1-\phi_R) + \phi_R + \chi_R \phi_R{}^2 + \frac{\rho_R V_1 \phi_R{}^{1/3}(1+2K^2)}{3M_C K^{4/3}} + \frac{(1+K)^2 + 2K^3}{2\left[(1+K)^3 - K^3\right]}\left\{\ln(1-\phi_P) + \phi_P + \chi_P \phi_P{}^2\right\} = 0$$

$$SI = 1 + \frac{\rho_S}{\omega_{gel}}\left\{\frac{\omega_R}{\rho_R}\left(\frac{1}{\phi_R} - 1\right) + \frac{\omega_{gel} - \omega_R}{\rho_P}\left(\frac{1}{\phi_P} - 1\right)\right\} \tag{C.3}$$

Where

ϕ_R Volume fraccion of rubber in the swollen rubber network
ϕ_P Volume fraccion of polystyrene in the swollen occluded polystyrene
χ_R Rubber-solvent interaction parameter
χ_P Polystyrene-solvent interaction parameter
ρ_R Density of grafted rubber
ρ_P Density of polystyrene
ρ_S Density of solvent
ω_{gel} Weight fraction of gel
ω_R Weight fraction of grafted and ungrefted corsslinked rubber in gel
V_1 Molar volume of the solvent
K Ratio of ϕ_R/ϕ_P
M_C Molecular weight between cross links

REFERENCES

1. M. Fischer and G.P. Hellmann, *Macromolecules*, **29**, 7 (1996).
2. A. Brydon, G.M. Burnett, and G.G. Cameron, *J. Polym. Sci. Polym. Chem. Ed*, **11**, 1 (1973).
3. D.A. Estenoz and G.R. Meira, *AICHE J.*, **44**, 2 (1998).
4. R. Albalak, Polymer Devolatilization, Taylor & Francis, New York (1996).
5. M.A. Villalobos, A.E. Hamielec, and P.E. Wood, *J. Appl. Polym. Sci.*, **42**, 629 (1991).
6. I.M. Gonzalez, G.R. Meira, and H.M. Oliva, *J. Appl. Polym. Sci.*, **59**, 1015 (1996).
7. R. Lopez-Negrete de la Fuente, J. Lopez-Rubio, A. Flores-Tlacuahuac, and E. Saldívar-Guerra, *Ind. Eng. Chem. Res.*, **45**(**5**), 1689 (2006).
8. D.A. Estenoz, G.R. Leal, Y.R. Lopez, M. Ha, Oliva, and G. R. Meira, *J. Appl. Polym. Sci*, **62**, 6 (1996).
9. J.R. Cerna, G. Morales, G.N. Eyler, and A.I. Carrizo, *J. Appl. Polym. Sci.*, **83**, 1 (2002).
10. P. Acuña, G. Morales, and R. Daz de Leon, *J. Appl. Polym. Sci.*, **114**, 3198 (2009).
11. M.J. Scorah, "Experimental and Modeling Investigation of a Novel Tetrafunctional Initiator in Free Radical Polymerization," Doctoral Thesis, University of Waterloo (2005).
12. D.A. Estenoz, E. Valdez, H.M. Oliva, and G.R. Meira, *J. Appl. Polym. Sci.*, **59**, 5 (1996).
13. F.M. Peng, *J Appl. Polym. Sci.*, **40**, 1289 (1990).
14. H.M. Oliva, G.R. Meira, D.A. Estenoz, and I.M. Gonzalez, *J. Appl. Polym. Sci.*, **74**, 1950 (1999).
15. E. Berkenwald, M.L. Laganá, J.M. Maffi, P. Acuña, G. Morales, and D. Estenoz, *J. Appl. Polym. Sci.*, **58**, 198 (2017). https://doi.org/10.1002/pen.24547.
16. V. Luciani, C.D.A. Estenoz, R. Meira, G, and H.M. Oliva, *Ind. Eng. Chem. Res.*, **44**, 22 (2005).
17. A. Flores-Tlacuahuac, L.T. Biegler, and E. Saldívar-Guerra, *Ind. Eng. Chem. Res.*, **44**(**8**), 2659 (2005).
18. B.J. Meister and A.E. Platt, *Ind. Eng. Chem. Res.*, **28**, 11 (1989).
19. R.J. Albalak, Z. Tadmor, and Y. Talmon, *AICHE J.*, **36**(**9**), 1313 (1990).
20. G. Astarita and P.L. Maffettone, *Macromol. Chem. Symp.*, **68**, 1 (1993).
21. R. Salazar, P. Ilundain, D. Alvarez, L. Da Cunha, J. Barandiaran, and M. Asua, *Ind. Eng. Chem. Res.*, **44**, 11 (2005).

22. J.D. Campbell, F. Teymour, and M. Morbidelli, *Macromolecules*, **36**(**15**), 5502 (2003).
23. J.D. Campbell, F. Teymour, and M. Morbidelli, *Macromolecules*, **36**(**15**), 5491 (2003).
24. D. Moscatelli, C. Cavallotti, and M. Morbidelli, *Macromolecules*, **39**(**26**), 9641 (2006).
25. M. Poutsma, *Polym. Degrad. Stab.*, **91**, 12 (2006).
26. H. Tobita, *J. Polym. Sci. B*, **39**, 391 (2001).
27. A.K. Tripathi, J.G. Tsavalas, and D.C. Sundberg, *Macromolecules*, **48**, 184 (2015).
28. M. Ali Parsa, I. Kozhan, M. Wulkow, and R.A. Hutchinson, *Macrom. Theory Simul.*, **23**, 207 (2014).
29. A.V. Castañeda Facio, Estudio de la Descomposicion Termica del Diperoxido de Pinacolona: Formacion de Oligomeros y Polímeros a base de Estireno con estructura *Defnida*, PhD thesis, Instituto Teconlogico de la Laguna (2007).
30. I.M. Maafa, J.B.P. Soares, and A. Elkamel, *Macromol. React. Eng.*, **1**, 364 (2007).
31. J.H. Duerksen, A.E. Hamielec, and J. Appl, *Polym. Sci. C Polym. Symp.*, **25**, 1 (2007).
32. A.W. Hui and A.E. Hamielec, *J. Appl. Polym. Sci.*, **16**, 3 (1972).
33. E. Berkenwald, L. Lagana, P. Acuña, G. Morales, and D. Estenoz, *Int. J. Chem. Reactor Eng.*, **14**, 1 (2016).
34. M. Wäckerlin and P. Nising, *Macromol. Symp.*, **259**, 1 (2007).
35. J.A. Biesenberger, Devolatilization of Polymers, Fundamentals – Equipment – Applications, Hanser Publishers, New York (1983).
36. D.S. Achilias and C. Kiparissides, *Macromolecules*, **25**, 14 (1992).
37. J.S. Vrentas, J.L. Duda, H.C. Ling, and J. Polym, *Sci. Polym. Phys. Ed.*, **22**, 459 (1984).
38. J.A. Biesenberger and D.H. Sebastian, Principles of Polymerization Engineering, Wiley, New York (1983).
39. R.E. Newman and R.H.M. Simon, A Mathematical Model of Devolatilization Promoted by Bubble Formation, Seventy-third Annual AIChE Meeting, Chicago (1980).
40. J.D. Stein, G. Fahrbach, and H. Adler, *Adv. Chem. Ser.*, **142**, 148 (1975).
41. H. Karam, L. Tien, and J. App, *Political Sci.*, **30**, 1969 (1985).
42. G. Morales, R. Diaz de Leon, P. Acuña, R. Flores Flores, and A. Montalvo Robles, *Polym. Eng. Sci.*, **46**, 1333 (2006).
43. J.R. Cerna Cortéz, Uso de peróxidos cíclicos multifuncionales como iniciadores de la polimerización, CIQA, México (2002)
44. D.C. De Kee, R.P. Chhabra, and P.J. Carreau, *AICHE J.*, **45**, 8 (1999).
45. G.N. Eyler, A.I. Cañizo, and R.K. Nesprias, *Química Nova*, **25**, 3 (2002).
46. Mexico Patent Request, MX/U/2016/0006600
47. E. Berkenwald, C. Spies, G. Morales, and D. Estenoz, *Polym. Eng. Sci.*, **55**, 1 (2014).
48. R. Diaz de Leon, G. Morales, P. Acuña, and F. Soriano, *Polym. Eng. Sci.*, **50**, 373 (2010).
49. S.J. Lee, H.G. Jeoung, and K.H. Ahn, *J. Appl. Polym. Sci.*, **89**, 3652 (2003).
50. N. Yaghini and P.D. Iedema, *Macromolecules*, **47**, 4851 (2014).